Triacetoneamine-derivates (EvAs) for CO_2-absorption from process gases

Elmar Kessler[a], Luciana Ninni[a], Dan Vasiliu[a], Amir Yazdani[a,1], Benjamin Willy[b], Rolf Schneider[c], Muhammad Irfan[c], Jörn Rolker[b], Erik von Harbou[a,*], Hans Hasse[a]

[a] *Laboratory of Engineering Thermodynamics (LTD), University of Kaiserslautern, P.O. Box 3049, 67653 Kaiserslautern, Germany*
[b] *Evonik Performance Materials GmbH, Rodenbacher Chaussee 4, 63457 Hanau-Wolfgang, Germany*
[c] *Evonik Technology & Infrastructure GmbH, Rodenbacher Chaussee 4, 63457 Hanau-Wolfgang, Germany*

Abstract

New amines for reactive absorption of CO_2 from process gases were investigated in a comprehensive experimental screening. All studied amines are derivates of triacetoneamine and differ only in the substituent of the triacetoneamine ring structure. The amines are abbreviated by the acronym EvA with a consecutive number, designating the derivate. About 50 EvAs were considered in this work from which 26 were actually synthesized and investigated in aqueous solution. The mass fraction of the amines in the unloaded solution was either $\tilde{w}^0_{\mathrm{EvA}} = 0.05$ g/g or $\tilde{w}^0_{\mathrm{EvA}} = 0.4$ g/g. The following properties were studied: solubility of CO_2, rate of absorption of CO_2, liquid-liquid and solid-liquid equilibrium, foaming behavior, dynamic viscosity, and acid constants. The nine most promising EvAs were evaluated with the NoVa short-cut method [1]. The method yields estimates for the specific energy demand and recirculation rate for a given purification task. Two typical purification tasks were considered: the CO_2-removal from natural gas and from synthesis gas, respectively. Some of the EvAs showed significantly improved performance compared to monoethanolamine (MEA) and a solvent-blend of methyl-diethanolamine and piperazine (MDEA/PZ).

Keywords:
CO_2-absorption, triacetoneamine-derivates (EvA), experimental screening of solvents, aqueous solution of amine

*Corresponding author
Email address: erik.vonharbou@mv.uni-kl.de (Erik von Harbou)
[1] Presently with Department of Plastics Engineering, University of Massachusetts Lowell, One University Avenue, Lowell, MA 01854, USA

Highlights

- Comprehensive experimental screening of a new class of solvents for CO_2-absorption.
- All solvents are aqueous solutions of triacetoneamine-derivates named EvAs.
- The EvAs systematically differ in the substituent of the triacetoneamine ring.
- Some EvAs show improved performance compared to MEA and MDEA/PZ.

1. Introduction

Aqueous solutions of amines are state of the art solvents for the reactive absorption of CO_2 from gaseous streams [2, 3, 4, 5]. The CO_2-absorption from flue gas to mitigate the climate change has received much attention in the recent past [6], but reactive CO_2-absorption also plays an important role in many established large-scale processes, like the purification of synthesis gas or natural gas [7, 8, 9, 10]. However, the energy demand for these separations is high and its reduction is an important goal, both economically and ecologically. The development of improved solvents for reactive absorption of CO_2 is one of the most important approaches to achieve this goal [11, 12]. Such a development usually starts with an experimental solvent screening. Bernhardsen and Knuutila have recently given a good review on reports of screenings of amine based solvents [13]. A survey of publications on such screenings is presented in Table 1. Most of the amines that were investigated in these screenings are commercially available. Only comparatively few research groups have synthesized new amines for the screening [14, 15, 16, 17, 18, 19, 20, 21, 22, 23]. Bubble cell apparatuses were used to investigate the CO_2-solubility and rate of absorption of CO_2 in most of these studies. Sometimes also the enthalpy of absorption of CO_2 or acid constants of the amines were measured. A few groups used temperature dependent fits of CO_2-solubility data to calculate the enthalpy of absorption of CO_2. Besides the experimental screenings, also group-contribution-based theoretical solvent screenings have been performed [24, 25].

In the present work, novel amines for the removal of CO_2 from process gases by reactive absorption were synthesized and investigated experimentally. All studied amines are derivates of triacetoneamine. They differ only in the substituent of the basic triacetoneamine ring structure. The amines are abbreviated by the acronym EvA. The number behind EvA designates the derivate. Physicochemical properties of two of these EvAs were thoroughly studied in previous works of our group [26, 27].

In the screening, about 50 EvAs were considered from which 26 were actually synthesized and investigated in aqueous solution. Seven apparatuses were used to study nine

properties of the solvents. The properties were chosen such as to characterize the solvents for industrial applications for CO_2-removal: CO_2-loading, rate of absorption of CO_2, acid constant, foaming behavior, solid precipitation, solubility in water, liquid-liquid demixing temperature, dynamic viscosity, and CO_2-solubility isotherms. The mass fraction of the EvAs in the unloaded aqueous solution was either $\tilde{w}^0_{\mathrm{EvA}} = 0.05$ g/g or $\tilde{w}^0_{\mathrm{EvA}} = 0.4$ g/g. Furthermore the NoVa short-cut method [1] was used to estimate the energy demand and recirculation rate of two typical purification tasks: the CO_2-removal from natural gas and from synthesis gas, respectively. The same procedures were applied for all amines. The results were compared to corresponding data for two amines that are widely used for CO_2-absorption: monoethanolamine (MEA) and a blend of methyl-diethanolamine (MDEA) and piperazine (PZ) with a mass ratio of 7:1 (MDEA/PZ). The aim of this comprehensive comparison is to evaluate the potential of the EvAs as an interesting class of aqueous solvents for the CO_2-absorption from process gases.

Table 1: Overview of publications on experimental screenings of aqueous solutions of amines for the CO_2-absorption.

author	investigated amines [2] / [3]	investigated solvents	experimental setups	investigated properties
Adeosun et al. (2013)[28]*	5 / -	5	2	f
Aronu et al. (2010)[29]	5 / -	8	1	a,b,e,f
Aronu et al. (2011)[30]*	9 / -	13	1	e,f
Aronu et al. (2013)[31]	8 / -	14	2	a,d,e,f
Brœder et al. (2012)[32]	7 / -	19	1	e,f
Chen et al. (2011)[33]	6 / -	7	1	e,f,g
Chen et al. (2011)[34]*	7 / -	8	2	c,e,f,g
Choi et al. (2014)[35]	5 / -	6	4	c,e,f,g
Chowdhury et al. (2009)[14]*	22 / 4	26	3	e,f,g
Chowdhury et al. (2011)[15]*	4 / 7	11	3	e,f,g
Chowdhury et al. (2013)[16]*	14 / 7	21	3	e,f,g
Conway et al. (2014)[19]*	3 / 30	33	2	e,f,h
Conway et al. (2014)[36]	7 / -	7	1	e,f,h
Du et al. (2016)[37]	22 / -	10	2	c,e,f
Dubois et al. (2013)[38]	10 / -	12	2	e,f
El Hadri et al. (2017)[39]	30 / -	30	3	a,e,f,g
Goto et al. (2011)[17]*	10 / 1	9	3	d,e,f,g

continued on next page

Table 1: continued from previous page

author	investigated amines [1] / [2]	investigated solvents	experimental setups	investigated properties
Goto et al. (2011)[18]	6 / 4	9	3	d,e,f,g
Hartono et al. (2017)[40]*	18 / -	18	2	c,e,f
Hook (1997)[21]	5 / 3	8	4	a,d,e,f
Kim et al. (2014)[41]*	6 / -	6	3	d,f,g
Luo et al. (2016)[42]	5 / -	10	2	e,f
Maneeintr et al. (2009)[22]*	1 / 5	6	1	f
Mergler et al. (2011)[43]*	5 / -	5	2	d,f
Muchan et al. (2017)[44]	4 / -	4	2	e,f,g
Muchan et al. (2017)[45]	9 / -	18	3	d,e,f,g
Puxty et al. (2009)[46]*	76 / -	76	2	e,f
Singh et al. (2007)[47]*	14 / -	14	1	a,e,f
Singh et al. (2009)[48]*	35 / -	35	1	a,e,f
Singh et al. (2009)[49]	33 / -	33	1	a,e,f
Singh et al. (2011)[50]*	27 / -	30	1	a,e,f
Singto et al. (2016)[23]	2 / 5	7	3	a,d,e,f,g
Wang et al. (2013)[51]	16 / -	16	1	e,f
Wang et al. (2013)[52]	15 / -	15	1	e,f
Yang et al. (2016)[20]	3 / 30	33	1	a,f
Zhang et al. (2017)[53]	8 / -	8	2	d,e,f
Zoghi et al. (2012)[54]	6 / -	16	1	e,f
This work (2019)	3 / 26	56	7	a,b,c,d,e,f,h

a: water solubility and/or solid precipitation, b: foaming behavior and/or liquid-liquid demixing, c: density and/or viscosity, d: information on chemical equilibrium e.g. pK-values or NMR, e: rate of absorption of CO_2, f: equilibrium CO_2-loading, g: calculated or measured enthalpy of absorption of CO_2, h: calculated energy demand of a purification task. *stated in Bernhardsen and Knuutila [13]. [1]commercially available, [2]synthesized for the screening.

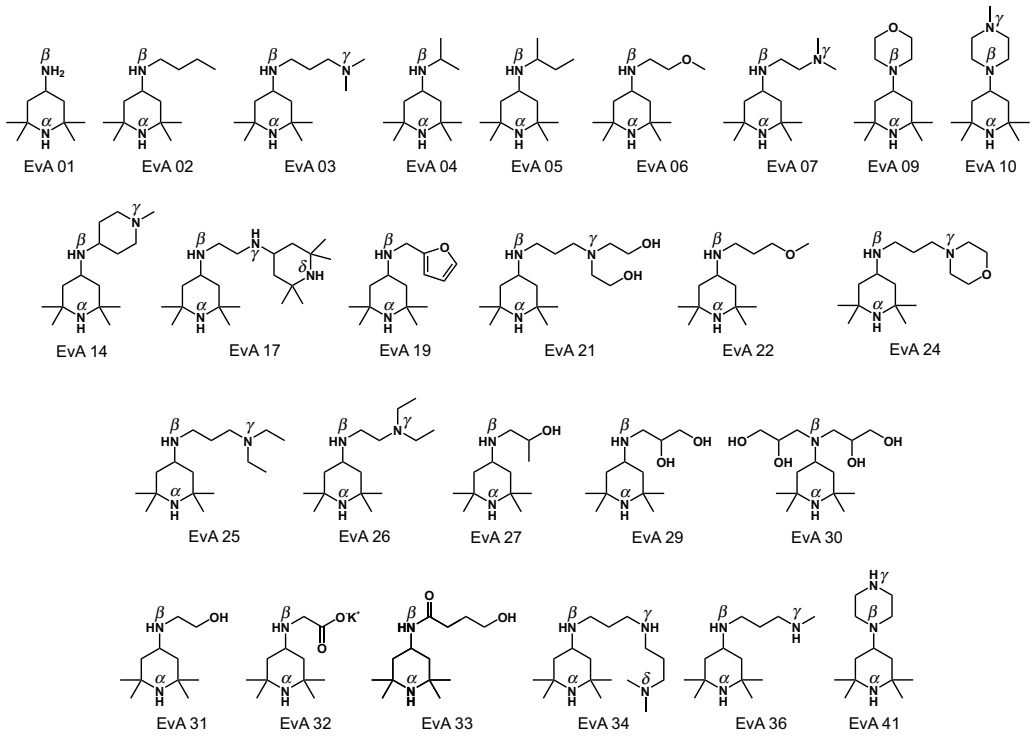

Figure 1: Chemical structures of the EvAs that were studied experimentally in the present work. Greek letters are used to label the different N-atoms.

2. Experiments

2.1. Chemicals

The investigated EvAs were provided by Evonik. They were synthesized by reductive amination using a noble metal catalyst [55, 56]. Either 2,2,6,6-tetramethyl-4-piperidone or 2,2,6,6-tetramethyl-4-amino-piperidine, respectively, was used as base chemical to which different substituents were added in the synthesis of EvA. After hydrogenation at elevated temperature and pressure, the EvAs were purified by vacuum distillation and filtration. The chemical structures of the synthesized EvAs are shown in Figure 1. Greek letters are used to designate the nitrogen atoms (N-atoms). The amount of the individual EvAs that were synthesized for the screening was between 80 g and 350 g.

The purified EvAs were analyzed by GC-MS, Karl-Fischer titration and $^{13}C\{^1H\}$ inverse gated NMR spectroscopy. The purities and major impurities are specified in Table 2. Also the molar mass M and the aggregate state of the synthesized EvAs at ambient pressure and 25 °C are reported in Table 2. In most cases purities larger than 96 mass % were reached. For EvA19, EvA22, EvA33, and EvA41, for which the purity was lower, the major impurities were elucidated by 2D NMR spectroscopy. They are also

stated in Table 2. EvA29 and EvA30 were obtained in a single synthesis and could not be separated. Therefore only the mixture EvA29/30 was investigated.

H_2O was purified by ion-exchange and filtration with a Siemens TWF/EI-Ion UV Plus water purification system. All other chemicals were purchased and used without further purification. Table 3 gives a survey of the chemicals that were used in the present work besides the EvAs.

Table 2: Properties and purities of the synthesized EvAs.

	M g/mol	AS	purity[a] mass %
EvA01	156.3	liquid	≥ 96
EvA02	212.4	liquid	≥ 96
EvA03	241.4	liquid	≥ 96
EvA04	198.4	liquid	≥ 96
EvA05	212.4	liquid	≥ 96
EvA06	214.4	liquid	≥ 96
EvA07	227.4	liquid	≥ 96
EvA09	226.4	solid	≥ 96
EvA10	239.4	solid	≥ 96
EvA14	253.4	liquid	≥ 96
EvA17	338.6	solid	≥ 96
EvA19	236.4	liquid	≥ 74[b]
EvA21	301.5	solid	≥ 96
EvA22	228.4	liquid	≥ 76[c]
EvA24	283.5	liquid	≥ 96
EvA25	269.4	liquid	≥ 96
EvA26	255.4	liquid	≥ 96
EvA27	214.4	solid	≥ 96
EvA29/30*	230.3 304.4	solid	≥ 96
EvA31	200.3	solid	≥ 96
EvA32	252.4	solid	≥ 96
EvA33	242.4	solid	≥ 84[d]
EvA34	298.5	liquid	≥ 96
EvA36	227.4	liquid	≥ 96

continued on next page

Table 2: continued from previous page

	M g/mol	AS	purity[a] mass %
EvA41	225.4	solid	≥ 87[e]

M: molar mass, AS: pure component aggregate state at ambient pressure and 25 ℃, *mixture of EvA29 (56 mass %) and EvA30 (44 mass %) with $M_{\mathrm{EvA29/30}}$ = 257.4 g/mol. [a]Impurities are mostly water and educts, [b]EvA01/triacetoneamine (7 mass %) and furan compounds (15 mass %), [c]EvA01/triacetoneamine (8 mass %) and 3-methoxy-propylamine (12 mass %), [d]EvA01/triacetoneamine (12 mass %), [e]piperazine (9 mass %).

Table 3: Chemicals that were used in the present work besides EvAs.

name (CAS)	source	purity
H_2O (7732-18-5)	Siemens TWF/EI-Ion UV Plus	0.99999 g/g
CO_2 (124-38-9)	Air Liquide	0.99995 mol/mol
$CO_2/O_2/N_2$ (-) 14/6/80 vol. %	Air Liquide	0.999 mol/mol
MEA (141-43-5)	Sigma-Aldrich	0.99 g/g
MDEA (105-59-9)	Sigma-Aldrich	0.99 g/g
PZ (110-85-0)	Sigma-Aldrich	0.99 g/g
1 M HCl (7647-01-0)	Carl Roth	0.998 mol/mol
1 M NaOH (1310-73-2)	Carl Roth	0.998 mol/mol
Titrisol pH-buffer (-)	Merck	

2.2. Sample preparation

Aqueous solutions of amines were prepared gravimetrically. The amount of amine and H_2O in the unloaded aqueous solution was determined with an accuracy of ± 1 mg. From this, the resulting mass fraction of the amine in the unloaded solvent $\tilde{w}^0_{\mathrm{amine}}$ is known with a relative expanded uncertainty of $U_r(\tilde{w}^0_{\mathrm{amine}}) = 0.001$ (0.99 level of confidence). The presence of impurities is not considered in the estimates of experimental uncertainties. In the symbol, the tilde refers to the overall amount of H_2O and amine without accounting the chemical reactions and their products.

The procedure of the CO_2-loading is described in the respective experimental sections. The content of CO_2 in the aqueous solutions of amine is reported as mass-related CO_2-loading $\tilde{X}_{CO_2}$, that is defined here as the ratio of the mass of CO_2 and the mass of the amine in the sample. Again, the tilde refers to the overall amounts without accounting the chemical reactions and their products.

The designation of the amines (EvA followed by a number, MEA, and MDEAZ/PZ) are used in the present work not only for identifying the amines. For brevity, they are also used for designating aqueous solutions that contain the respective amine. This short-cut notation is used mainly in the results section and only where the context excludes any confusion with the pure amines.

2.3. Qualitative investigations

2.3.1. Solubility of EvAs in water

The solubility of EvAs in H_2O was investigated at two mass fractions of EvA in the unloaded solvent: $\tilde{w}^0_{EvA} = 0.05$ g/g and $\tilde{w}^0_{EvA} = 0.4$ g/g. After mixing the EvA with H_2O, the solution was stirred for 24 hours, and then stored for 7 days at 25 ℃ and ambient pressure. If no solids were visible after that period, the EvAs were classified as soluble in H_2O. Otherwise they were classified as poorly soluble. Each experiment was performed once.

The expanded uncertainty of the mass fraction of EvA in the unloaded solvent is the same as specified in Section 2.2. The temperature was controlled by air conditioning. The expanded uncertainty of the temperature measurement is $U(t) = 1$ ℃ (0.99 level of confidence).

2.3.2. Foaming behavior

The foaming behavior of CO_2-loaded aqueous solutions of EvA was assessed by comparing foam heights above 100 g of aqueous solutions of amines, through which a stream of $\dot{V} = 100$ Ncm^3/min of pure CO_2 at a pressure of $p_{CO_2} = 1$ bar was bubbled inside a cylinder that had an inner diameter of 3.2 cm. The flow-saturator setup that was used for the investigation was the same as in a previous work of our group [26]. Therefore, no further details on the setup are given here. The mass fraction of amine in the unloaded solvent was $\tilde{w}^0_{EvA} = 0.4$ g/g. The temperature was 40 ℃. The foam heights were observed for 4 hours. All aqueous solutions of amines reached their equilibrium CO_2-loading within that period. The maximum foam height that was observed for at least 5 minutes during the experiment was recorded and is considered here as the result. An aqueous solutions of MEA with the same mass fraction of amine in the unloaded solvent was taken as reference. The foam height of the reference was about 7 cm. The fluctuation within the 5 minutes

was about 2 cm. The foam heights of the EvAs are roughly classified as higher, equal, or lower compared to the reference. The volume flow was measured with a calibrated G51 thermal volume flow meter from MKS. The pressure was measured with a calibrated high precision pressure transducer from WIKA. The temperature of the thermostatting bath, that was used for thermostatting the cylinder, was measured with a calibrated Pt100. Each experiment was performed once.

The expanded uncertainty of the mass fraction of EvA in the unloaded solvent is the same as specified in Section 2.2. The standard uncertainty of the volume flow of CO_2 is $u(\dot{V}) = 10\ \mathrm{Ncm^3/min}$. The expanded uncertainty of the temperature measurement in the thermostatting bath is $U(t) = 1$ ℃ (0.99 level of confidence). The standard uncertainty of the partial pressure of CO_2 inside the cylinder is $u(p_{CO_2}) = 25$ mbar.

2.3.3. Solid precipitation

The occurrence of solid precipitation in CO_2-loaded aqueous solutions of EvA was investigated by visual analysis of samples with two different mass fractions of EvA in the unloaded solvent: $\tilde{w}^0_{\mathrm{EvA}} = 0.05$ g/g and $\tilde{w}^0_{\mathrm{EvA}} = 0.4$ g/g. The samples were taken while the aqueous solutions of EvAs were loaded with CO_2. The samples with $\tilde{w}^0_{\mathrm{EvA}} = 0.05$ g/g were taken during the bubble cell experiments that are described in Section 2.4.4. The samples with $\tilde{w}^0_{\mathrm{EvA}} = 0.4$ g/g were taken from the flow-saturator experiments that are described in Section 2.3.2. All samples were stored in glass vials for 7 days at 25 ℃. Zeolite chips were added to the samples as crystallization germs. A visual analysis of the samples after 7 days revealed if solid precipitation occurred. If at least one sample of a CO_2-loaded aqueous solution of a given EvA revealed solid precipitation, it was classified as "'solid precipitating"'. Each experiment was performed once.

The expanded uncertainty of the mass fraction of EvA in the unloaded solvent is the same as specified in Section 2.2. The temperature was controlled by air conditioning. The expanded uncertainty of the temperature measurement is $U(t) = 1$ ℃ (0.99 level of confidence). The pressure inside the sample vials was not measured as it has no significant influence on the occurrence of solid precipitation.

2.4. Quantitative investigations

2.4.1. Density and dynamic viscosity

The density of unloaded aqueous solutions of EvAs was measured in a calibrated oscillating U-tube densimeter (Anton Paar DMA 4500 M). The dynamic viscosity of unloaded aqueous solutions of EvA was measured in a calibrated falling sphere viscosimeter (HAAKE type 800-0197). Both properties were investigated with a mass fraction of EvA

in the unloaded solvent of $\tilde{w}^0_{\mathrm{EvA}} = 0.4$ g/g at 25 ℃ and ambient pressure. The temperature was measured with a calibrated Pt100. Each aqueous solution of EvA was measured six times. The arithmetic mean values of the measured density and dynamic viscosity are reported here as the result.

The standard uncertainty of the measured density and dynamic viscosity is calculated from the standard deviation of the repeated measurements and the standard uncertainty from calibration. The standard uncertainty of the density is $u(\rho) = 0.01$ g/cm^3. The standard uncertainty of the dynamic viscosity is reported in the results for each EvA, separately. The expanded uncertainty of the mass fraction of EvA in the unloaded solvent is the same as specified in Section 2.2. The expanded uncertainty of the temperature measurement is $U(t) = 1$ ℃ (0.99 level of confidence).

2.4.2. Demixing temperature

The liquid-liquid demixing temperature of unloaded aqueous solutions of EvAs was investigated by visual analysis of samples that were thermostatted in an oven. The mass fraction of EvA in the unloaded solvent was always $\tilde{w}^0_{\mathrm{EvA}} = 0.4$ g/g in the experiments. Glass vials that contained about 15 ml of the unloaded aqueous solutions of EvAs were subjected to a temperature program in which, after keeping the temperature constant for 2 hours, the temperature was increased in steps of 5 ℃. A visual analysis of the samples was performed prior to each temperature increase and any occurrence of a liquid-liquid demixing was recorded. The mean temperature between the recorded demixing temperature and the previous temperature, where no demixing was observed, is reported here as the demixing temperature. The temperature inside the oven was measured with a calibrated Pt100 thermometer. Each experiment was performed twice.

The expanded uncertainty of the measured demixing temperature is calculated from the temperature step size and the expanded uncertainty of the temperature measurement and is $U(t_{\mathrm{demix}}) = 2.7$ ℃ (0.99 level of confidence). The expanded uncertainty of the mass fraction of EvA in the unloaded solvent is the same as specified in Section 2.2. The pressure inside the glass vials was not measured but has no significant influence on the demixing temperature.

2.4.3. pK-values

The molal activity-based pK-values of highly diluted aqueous solutions of EvAs were determined by titration experiments at 20 ℃, 40 ℃, and 60 ℃. The equipment and the way the experiments were conducted and evaluated were the same as in a previous work of our group [57]. Therefore, no details are given here. The pH-value was measured with a Metrohm LL Unitrode. The pH-electrode also contained a calibrated Pt1000 that was

used for the temperature measurement. The pH-electrode was calibrated with five buffer solutions at pH = 2, 6, 8, 10, and 12 before and after every temperature change. Each experiment was performed once.

The standard uncertainty of the measured pK-value is calculated from the standard deviation of repeated experiments of previous works of our group [26, 57] and from the standard uncertainty of the calibration and is $u(\mathrm{p}K) = 0.15$ on the pH-scale. The expanded uncertainty of the temperature measurement is $U(t) = 1$ ℃ (0.99 level of confidence). All titrations were performed at ambient pressure.

2.4.4. Initial rate of absorption and equilibrium CO_2-loading

The initial rate of absorption and equilibrium CO_2-loading was measured in a bubble cell, which is schematically shown in Figure 2. A gas stream of 1000 Ncm^3/min, containing 14 vol % CO_2, 6 vol % O_2 and 80 vol % N_2 from a gas cylinder, was bubbled through 150 g of an aqueous solution of amine with a mass fraction of amine in the unloaded solvent of $\tilde{w}^0_{\mathrm{amine}} = 0.05$ g/g. The total pressure was kept constant at 1 bar. The aqueous solution of amine was thermostatted by a surrounding bath. The experiments were performed at 40 ℃ and 100 ℃. A water-cooled condenser was installed above the bubble cell. The volume flow was measured with a calibrated rotameter from Yokogawa. The pressure was measured with a calibrated pressure transducer from WIKA. The temperature of the thermostatting bath was measured with a calibrated Pt100 thermometer. The mole fraction of CO_2 leaving the bubble cell was measured by a calibrated Ansyco-G100 infrared (IR) spectrometer. A sketch of a typical resulting IR-signal is shown in the upper right part of Figure 2. From the IR-signal, the loading-curve was calculated. A sketch of a loading-curve is shown in the lower right part of Figure 2. The loading-curve was calculated by integrating the amount of CO_2 that was captured in the bubble cell over time. That amount was found from the difference between the inlet and the outlet mole fraction of CO_2 of the bubble cell. N_2 and O_2 were assumed to be inert.

Two results were obtained from the loading-curve: the equilibrium CO_2-loading $\tilde{X}_{\mathrm{CO_2}}$ and the initial rate of absorption RA. The equilibrium CO_2-loading $\tilde{X}_{\mathrm{CO_2}}$ was calculated by dividing the total amount of CO_2 that was captured in one experiment by the amount of amine in the bubble cell, which was known from sample preparation. The equilibrium CO_2-loading was investigated at 40 ℃ and 100 ℃. The initial rate of absorption RA was determined from a linear fit of the initial 16 minutes of the loading curve and was only evaluated at 40 ℃. Each experiment was performed once.

The experimental setup and procedure was tested with aqueous solutions of MEA. The relative standard uncertainty of the measured equilibrium CO_2-loading is calculated from the standard uncertainty of the IR-calibration and the standard deviation of the repeated

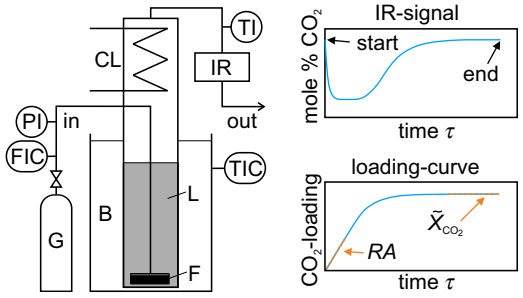

Figure 2: Experimental setup of the bubble cell. G: feed gas, L: aqueous solution of amine, F: dispersion frit, B: thermostatting bath, CL: water-cooled condenser, IR: infrared spectrometer for measuring the CO_2 concentration. The diagrams are explained in the text.

testings with MEA and is $u_r(\tilde{X}_{CO_2}) = 0.05$. This relative standard uncertainty is also taken as an estimate for the relative standard uncertainty of the measured initial rate of absorption: $u_r(RA) = 0.05$. The standard uncertainty of the initial rate of absorption includes variations in the volume flow. The standard uncertainty of the partial pressure of CO_2 is $u(p_{CO_2}) = 5$ mbar. The expanded uncertainty of the mass fraction of EvA in the unloaded solvent is the same as specified in Section 2.2. The expanded uncertainty of the temperature measurement in the thermostatting bath is $U(t) = 1$ ℃ (0.99 level of confidence).

2.4.5. CO_2-solubility isotherms

The CO_2-solubility in aqueous solutions of EvAs with a mass fraction of EvA in the unloaded solvent of $\tilde{w}^0_{EvA} = 0.4$ g/g was measured by head space gas chromatography at 40 ℃ and 100 ℃. The equipment was the same as in previous works of our group [57, 58, 59] and is therefore not described here in detail. For the screening, the samples were prepared in stainless steel cells that were directly used in the head space gas chromatography apparatus. The amount of aqueous solution of EvA and CO_2 was determined by differential weighing. The CO_2-loading was determined from the weighed amounts of CO_2 and EvA. The partial pressure of CO_2 in the gas phase above the sample inside the cell was determined by gas chromatography. The gas chromatograph (Agilent, type 6890) was equipped with a capillary column (J&M Scientific, type G5-Q, 30 m, 0.32 mm i.d.) and a thermal conductivity detector. For calibrating the partial pressure of CO_2, the sample cells were filled with CO_2 at pressures ranging from 50 to 1500 mbar. The calibration was performed before and after each temperature change. The sample cells were thermostatted with a bath, surrounding the cells. The temperature was measured with calibrated platinum resistance thermometer in the surrounding thermostatting bath. Each sample was measured once.

Results for aqueous solutions of EvA34 from head space gas chromatography experiments of this work were compared to a corresponding data set from a previous work of our group with the same apparatus [57]. The results are in good agreement. The relative standard uncertainty of the measured partial pressure of CO_2 is calculated from the standard deviation of the comparison with the previous experiments and the standard uncertainty of the calibration and is $u_r(p_{CO_2}) = 0.08$. The expanded uncertainty of the mass fraction of EvA in the unloaded solvent is the same as specified in Section 2.2. The accuracy of the weighing of CO_2 was ± 1 mg. The resulting relative expanded uncertainty of the CO_2-loading is $U_r(\tilde{X}_{CO_2}) = 0.01$ (0.99 level of confidence). The expanded uncertainty of the temperature measurement in the thermostatting bath is $U(t) = 0.1$ ℃ (0.99 level of confidence).

3. Results

3.1. Solubility in water, solid precipitation, and foaming behavior

Table 4 shows the results that were obtained in the qualitative assessment of the solubility in water of unloaded aqueous solutions of amines, as well as of solid precipitation and foaming behavior of CO_2-loaded aqueous solutions of amines.

All EvAs are soluble in water at a mass fraction of amine in the unloaded solvent of $\tilde{w}^0_{\text{amine}} = 0.05$ g/g. At $\tilde{w}^0_{\text{amine}} = 0.4$ g/g, all EvAs except EvA14, EvA17, EvA32 and EvA33 are soluble in water. From these, EvA14 is the only which is liquid as the pure component but forms solids in aqueous solution at $\tilde{w}^0_{\text{amine}} = 0.4$ g/g. EvA17 has the highest molar mass of all studied amines. EvA32 is the only amino-acid, and EvA33 is the only amide in the study. The aqueous solution of EvA19 is a crude-oil-like opaque black liquid. All other aqueous solutions of EvA are translucent reddish liquids.

In the experiments in the bubble cell (cf. Section 2.4.4), only the CO_2-loaded aqueous solutions of EvA19 showed solid precipitation at a mass fraction of amine in the unloaded solvent of $\tilde{w}^0_{\text{amine}} = 0.05$ g/g. EvA19 is the only EvA that contains an aromatic furan-ring. At $\tilde{w}^0_{\text{amine}} = 0.4$ g/g, solid precipitation was observed in the flow-saturator experiments (cf. Section 2.3.2) for 12 of the 21 EvAs that are soluble in water. No solid precipitation was observed for EvA03, EvA06, EvA09, EvA21, EvA24, EvA29/30, EvA34, and EvA36. EvA25 also passed the 7 days test used here for the classification of solid precipitation and was therefore classified as not solid precipitating. However, after several month, solids were found in some of the CO_2-loaded samples of EvA25. A similar behavior was observed for EvA02 in a previous work of our group [26]. A pattern to establish a connection between the molecular structure of the EvAs and the occurrence of solid precipitation was not found in the present data. However, the results clearly show that

the probability of solid precipitation increases with increasing mass fraction of amine in the unloaded solvent.

The observed foam height of the reference MEA was about 7 cm in the experiments. EvA03, the mixtures EvA29/30 and MDEA/PZ showed similar foam heights. For all other studied EvAs, a distinctly lower foam height was observed. Less foaming is advantageous for operability of absorption/desorption processes.

Table 4: Experimental results of the qualitative assessment of the solubility in water, solid precipitation, and foaming behavior of unloaded and CO_2-loaded aqueous solutions of amines from the present work.

	solubility in water		solid precipitation		foam height
$\tilde{w}^0_{\text{amine}}$ / g/g	0.05	0.4	0.05	0.4	0.4
t / ℃	25	25	25	25	40
CO_2-loading	no	no	yes	yes	yes
MEA	soluble	soluble	no	no	reference
MDEA/PZ	soluble	soluble	no	no	similar
EvA01	soluble	soluble	no	yes	lower
EvA02	soluble	soluble	no	yes	lower
EvA03	soluble	soluble	no	no	similar
EvA04	soluble	soluble	no	yes	lower
EvA05	soluble	soluble	no	yes	lower
EvA06	soluble	soluble	no	no	lower
EvA07	soluble	soluble	no	yes	lower
EvA09	soluble	soluble	no	no	lower
EvA10	soluble	soluble	no	yes	lower
EvA14	soluble	poor	no	[a]	[a]
EvA17	soluble	poor	no	[a]	[a]
EvA19	soluble	soluble	yes	yes	lower
EvA21	soluble	soluble	no	no	lower
EvA22	soluble	soluble	no	yes	lower
EvA24	soluble	soluble	no	no	lower
EvA25	soluble	soluble	no	no[b]	lower
EvA26	soluble	soluble	no	yes	lower

continued on next page

Table 4: continued from previous page

	solubility in water		solid precipitation		foam height
$\tilde{w}^0_{\text{amine}}$ / g/g	0.05	0.4	0.05	0.4	0.4
t / ℃	25	25	25	25	40
CO_2-loading	no	no	yes	yes	yes
EvA27	soluble	soluble	no	yes	lower
EvA29/30	soluble	soluble	no	no	similar
EvA31	soluble	soluble	no	yes	lower
EvA32	soluble	poor	no	[a]	[a]
EvA33	soluble	poor	no	[a]	[a]
EvA34	soluble	soluble	no	no	lower
EvA36	soluble	soluble	no	no	lower
EvA41	soluble	soluble	no	yes	lower

$\tilde{w}^0_{\text{amine}}$: mass fraction of amine in the unloaded solvent with the relative expanded uncertainty $u_r(\tilde{w}^0_{\text{amine}}) = 0.001$ (0.99 level of confidence), t: temperature with the expanded uncertainty $U(t) = 1$ ℃ (0.99 level of confidence). [a]not available due to poor solubility in H_2O. [b]EvA25 passed the 7 days test but showed solid precipitation after several month.

3.2. Density, dynamic viscosity and demixing temperature

Table 5 shows the quantitative results of the experimental studies of the density ρ, the dynamic viscosity η, and the liquid-liquid demixing temperature t_{demix}.

The density of the investigated aqueous solutions of EvAs at 25 ℃ differs between ρ = 0.978 g/cm^3 for EvA05 and ρ = 1.027 g/cm^3 for EvA29/30 and EvA19.

The dynamic viscosity of the aqueous solutions of EvAs at 25 ℃ differs between η = 7.9 mPa·s for EvA01 and η = 22.1 mPa·s for EvA34. As expected, in general, the dynamic viscosity increases with increasing molar mass. Most of the studied aqueous solutions of EvA show higher dynamic viscosities than the aqueous solutions of MEA and MDEA/PZ. Higher viscosities are disadvantageous for the mass transfer.

The lowest liquid-liquid demixing temperature was observed for EvA02 at t_{demix} = 42.5 ℃. The demixing temperature increases with increasing ratio of polar groups (hydroxy, ether, ketone, amino) to unpolar groups (hydrocarbons) in the molecule. No demixing was observed for EvAs that contain hydroxy-groups (EvA21, EvA27, EvA29/30, EvA31),

primary amino-groups (EvA01), or unhindered secondary amino-groups (EvA34, EvA36, EvA41), respectively.

Table 5: Density, dynamic viscosity, and liquid-liquid demixing temperature of unloaded aqueous solutions of EvAs with $\tilde{w}^0_{\text{amine}} = 0.4$ g/g. Experimental results from the present work.

	ρ	η	t_{demix}
	g/cm^3	mPa·s	℃
MEA	1.016	3.7 ± 1.3	no[a]
MDEA/PZ	1.033	5.8 ± 1.6	no[a]
EvA01	0.999	7.9 ± 1.6	no[a]
EvA02	0.984	11.6 ± 1.5	42.5
EvA03	0.999	15.5 ± 2.0	107.5
EvA04	0.986	9.1 ± 2.0	62.5
EvA05	0.978	10.4 ± 1.8	47.5
EvA06	1.006	8.6 ± 1.8	117.5
EvA07	1.000	14.7 ± 2.0	122.5
EvA09	1.024	9.3 ± 1.0	82.5
EvA10	1.018	17.5 ± 2.4	92.5
EvA19	1.027	9.3 ± 1.8	72.5
EvA21	1.034	11.7 ± 2.0	no[a]
EvA22	0.998	9.8 ± 1.8	87.5
EvA24	1.024	14.6 ± 2.0	127.5
EvA25	0.992	17.4 ± 2.2	67.5
EvA26	0.995	16.1 ± 2.0	72.5
EvA27	1.015	14.8 ± 2.3	no[a]
EvA29/30	1.027	13.8 ± 2.1	no[a]
EvA31	1.021	11.6 ± 1.9	no[a]
EvA34	1.002	22.1 ± 2.4	no[a]
EvA36	1.004	14.0 ± 2.0	no[a]
EvA41	1.025	9.4 ± 1.8	no[a]

continued on next page

Table 5: continued from previous page

	ρ	η	t_{demix}
	g/cm^3	mPa·s	℃

$\tilde{w}^0_{\mathrm{amine}}$: mass fraction of amine in the unloaded solvent with the relative expanded uncertainty $u_r(\tilde{w}^0_{\mathrm{amine}}) = 0.001$ (0.99 level of confidence), ρ: density at $t = 25$ ℃ with the standard uncertainty $u(\rho) = 0.01$ g/cm^3 and the expanded uncertainty $U(t) = 1$ ℃ (0.99 level of confidence) η: dynamic viscosity at $t = 25$ ℃ with the intervals representing the standard uncertainty $u(\eta)$ and the expanded uncertainty $U(t) = 1$ ℃ (0.99 level of confidence), t_{demix}: liquid-liquid demixing temperature with the expanded uncertainty $U(t_{\mathrm{demix}}) = 2.7$ ℃ (0.99 level of confidence). [a]no liquid-liquid demixing observed below 130 ℃.

3.3. pK-values

The molal activity-based pK-values, which were determined from titration experiments of highly diluted aqueous solutions of EvAs at 20 ℃, 40 ℃, and 60 ℃, are listed in Table 6. In Table 6, the Greek letters indicate to which N-atom the pK-value corresponds (cf. Figure 1). For the mixture EvA29/30 and for EvA41, which was contaminated with piperazine, no reliable information on the pK-values could be obtained from the titration curves.

The highest pK-value was assigned to the α-N-atom for all EvAs. Literature data [26, 57, 60] and the positive inductive effect of the surrounding 2,2,6,6-tetramethyl-piperidine-ring support this assignment. The second highest pK-value was assigned to the N-atom that has the highest spatial distance to the α-N-atom. This is the γ-N-atom for EvAs that contain three N-atoms (EvA03, EvA07, EvA10, EvA14, EvA21, EvA24, EvA25, EvA26, EvA36), and the δ-N-atom for EvAs that contain four N-atoms (EvA17, EvA34). Literature data for similar amines support these assignments [57, 60, 61]. The third highest pK-value of EvA34 was assigned to the β-N-atom, according to literature [57]. The third highest pK-value of EvA17 was assigned to the γ-N-atom. For EvA17, due to the lower pK-value of the δ-N-atom, compared to the α-N-atom, the δ-N-atom is less protonated than the α-N-atom. Hence, the γ-N-atom is less influenced by protonated N-atoms nearby than the β-N-atom, and is thus expected to have a higher pK-value than the β-N-atom.

The pK-values are strongly influenced by the substituents. As expected, the β-N-atom that links the substituent to the piperidine-ring is influenced more stronlgy by the nature of the substituent than the α-N-atom. However, also the α-N-atom is influenced by the substituent, despite the spatial separation. Substituents that contain oxygen-atoms (marked with an asterisk in Table 6) reduce the pK-values. This is due to the negative inductive effect of oxygen-atoms. An exception is EvA33, where the pK-value of the β-N-atom is remarkably high. EvA33 contains a secondary amide group. Amides are reported to have high pK-values [62, 63]. In general, higher pK-values are advantageous for the absorption of CO_2. EvA03, EvA17, EvA25, EvA34, and EvA36 as well as EvA33 show high pK-values. In that group of EvAs only EvA33 contains an oxygen-atom.

Table 6: pK-values of the investigated EvAs. Experimental results from the present work. Greek letters indicate the corresponding N-atom according to the designation in Figure 1.

	pK-values											
t / ℃	20				40				60			
EvA01	10.8^{α}	8.2^{β}			10.3^{α}	7.7^{β}			9.7^{α}	7.2^{β}		
EvA02	10.9^{α}	8.3^{β}			10.4^{α}	7.7^{β}			9.8^{α}	7.3^{β}		
EvA03	10.8^{α}	9.4^{γ}	6.9^{β}		10.2^{α}	8.9^{γ}	6.4^{β}		9.7^{α}	8.4^{γ}	5.9^{β}	
EvA04	10.8^{α}	8.3^{β}			10.3^{α}	7.7^{β}			9.7^{α}	7.3^{β}		
EvA05	10.9^{α}	8.3^{β}			10.3^{α}	7.8^{β}			9.6^{α}	7.3^{β}		
EvA06*	10.6^{α}	7.5^{β}			10.0^{α}	6.9^{β}			9.4^{α}	6.6^{β}		
EvA07	10.6^{α}	8.8^{γ}	4.8^{β}		10.1^{α}	8.4^{γ}	4.5^{β}		9.5^{α}	8.0^{γ}	4.1^{β}	
EvA09*	10.4^{α}	5.7^{β}			9.8^{α}	5.6^{β}			9.2^{α}	5.1^{β}		
EvA10	10.4^{α}	7.7^{γ}	2.6^{β}		9.9^{α}	7.5^{γ}	2.5^{β}		9.1^{α}	7.0^{γ}	2.4^{β}	
EvA14	10.7^{α}	9.1^{γ}	5.8^{β}		10.1^{α}	8.7^{γ}	5.4^{β}		9.5^{α}	8.2^{γ}	5.1^{β}	
EvA17	10.9^{α}	9.9^{δ}	7.5^{γ}	4.6^{β}	10.4^{α}	9.4^{δ}	7.1^{γ}	4.2^{β}	9.7^{α}	8.8^{δ}	6.6^{γ}	3.8^{β}
EvA19*	10.5^{α}	7.0^{β}			9.9^{α}	6.5^{β}			9.3^{α}	6.0^{β}		
EvA21*	10.7^{α}	8.6^{γ}	6.2^{β}		10.2^{α}	8.2^{γ}	5.9^{β}		9.6^{α}	7.7^{γ}	5.4^{β}	
EvA22*	10.6^{α}	7.9^{β}			10.1^{α}	7.5^{β}			9.5^{α}	6.9^{β}		
EvA24*	10.8^{α}	8.0^{γ}	6.0^{β}		10.1^{α}	7.6^{γ}	5.7^{β}		9.4^{α}	7.1^{γ}	5.3^{β}	
EvA25	10.9^{α}	9.8^{γ}	6.7^{β}		10.3^{α}	9.3^{γ}	6.4^{β}		9.7^{α}	8.7^{γ}	5.9^{β}	
EvA26	10.6^{α}	9.3^{γ}	4.9^{β}		10.1^{α}	8.9^{γ}	4.5^{β}		9.6^{α}	8.4^{γ}	4.2^{β}	
EvA27*	10.6^{α}	7.6^{β}			10.0^{α}	7.1^{β}			9.5^{α}	6.7^{β}		
EvA31*	10.5^{α}	7.5^{β}			10.0^{α}	7.1^{β}			9.5^{α}	6.7^{β}		

continued on next page

Table 6: continued from previous page

	pK-values											
t / ℃	20				40				60			
EvA32*	10.6^{α}	7.6^{β}			10.1^{α}	7.3^{β}			9.5^{α}	6.9^{β}		
EvA33*	10.5^{α}	9.4^{β}			9.9^{α}	9.1^{β}			9.4^{α}	8.2^{β}		
EvA34	10.9^{α}	9.8^{δ}	8.3^{β}	6.7^{γ}	10.3^{α}	9.3^{δ}	7.7^{β}	6.2^{γ}	9.8^{α}	8.9^{δ}	7.5^{β}	5.9^{γ}
EvA36	11.0^{α}	9.9^{γ}	6.9^{β}		10.4^{α}	9.4^{γ}	6.5^{β}		9.9^{α}	8.8^{γ}	6.0^{β}	

*EvAs that contain oxygen-atoms. pK-values on the molal activity based pH-scale with the standard uncertainty $u(\mathrm{p}K) = 0.15$. t: temperature with the expanded uncertainty $U(t) = 1$ ℃ (0.99 level of confidence).

3.4. Equilibrium CO_2-loading

Figure 3 shows equilibrium CO_2-loadings of the studied aqueous solutions of amines $\tilde{X}_{CO_2}$ at 40 ℃ and 100 ℃ that were obtained in bubble cell experiments at a partial pressure of CO_2 of $p_{CO_2} = 140$ mbar. The mass fraction of amine in the unloaded solvent was always $\tilde{w}^0_{\mathrm{amine}} = 0.05$ g/g in these experiments. This low mass fraction was chosen to avoid solid precipitation. The results are displayed in descending order of the difference between the equilibrium CO_2-loading at 40 ℃ and 100 ℃. The value of this difference $\Delta\tilde{X}_{CO_2}$ is given in the Figure as well. The data are divided into three groups: EvAs that contain oxygen-atoms, EvAs that do not contain oxygen-atoms, and the references MEA and MDEA/PZ. The corresponding experimental numerical data are given in the Appendix.

In general, EvAs that do not contain oxygen-atoms show higher $\tilde{X}_{CO_2}$ at 40 ℃ than EvAs that contain oxygen-atoms. Oxygen-atoms lower the basicity (cf. Section 3.3), which consequently lowers the equilibrium CO_2-loading. But also $\Delta\tilde{X}_{CO_2}$ is in general larger for EvAs that do not contain oxygen-atoms than for EvAs that contain oxygen-atoms. This might be related to the temperature dependency of the pK-values: high pK-values decrease stronger with increasing temperature, than low pK-values (cf. Section 3.3).

However, also exceptions to this general relation between the equilibrium CO_2-loading and the pK-value were found. The amide EvA33 and the amino-acid EvA32, for example, show much lower $\tilde{X}_{CO_2}$ and $\Delta\tilde{X}_{CO_2}$ than expected from their pK-values. Another exception is EvA01, for which $\Delta\tilde{X}_{CO_2}$ is very small compared to other EvAs with similar high $\tilde{X}_{CO_2}$. Here, the different functional groups (e.g. amide, amino-acid, primary-,

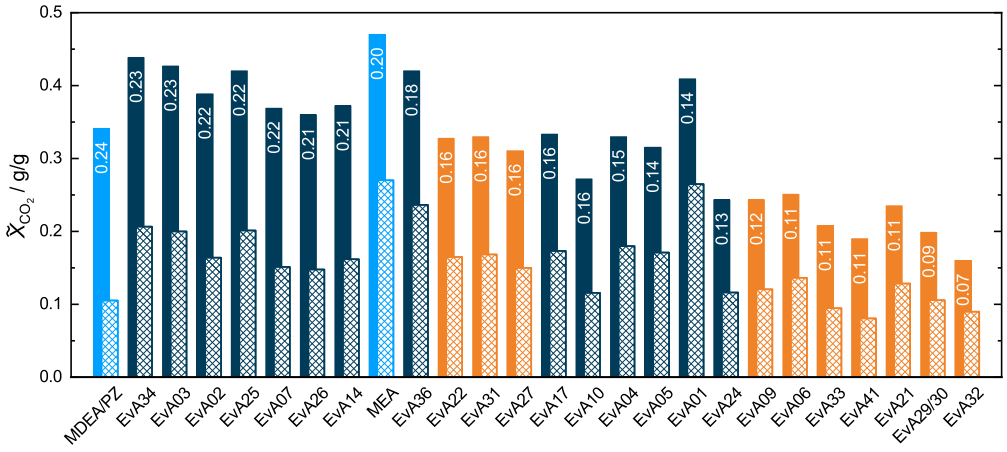

Figure 3: Equilibrium CO_2-loading for aqueous solutions of amines with $\tilde{w}^0_{\text{amine}} = 0.05$ g/g at $p_{CO_2} =$ 140 mbar. Experimental results from bubble cell experiments of this work. ■: 40 °C, ⊠: 100 °C. Orange: EvAs that contain oxygen-atoms, grey: EvAs that do not contain oxygen-atoms, blue: references. The number indicates the difference between the equilibrium CO_2-loadings at 40 °C and 100 °C $\Delta\tilde{X}_{CO_2}$. The results are displayed in order of descending numbers of $\Delta\tilde{X}_{CO_2}$.

secondary-, tertiary N-atoms, etc.) reveal their strong influence on the results. We refrain from a more detailed discussion of the influencing factors, as more data would be required for further conclusions, e.g. on the equilibrium constants of the chemical reactions in the studied systems.

The largest $\Delta\tilde{X}_{CO_2}$ is found for the reference MDEA/PZ. However, $\Delta\tilde{X}_{CO_2}$ for several of the EvAs (EvA34, EvA03, EvA02, EvA25, EvA07, EvA26, and EvA14) are similar and surpass that of the reference MEA. They are all part of the group of EvAs that do not contain oxygen-atoms. They show higher $\tilde{X}_{CO_2}$ than MDEA/PZ but lower $\tilde{X}_{CO_2}$ than MEA at 40 °C and 100 °C, respectively. It is remarkable that five out of these seven EvAs (EvA03, EvA07, EvA14, EvA25, and EvA26) have very similar molecular structure and vary only in the length of the alkane-parts of the substituents of the tertiary γ-N-atom.

3.5. Initial rate of absorption of CO_2

Figure 4 shows the experimental results for the initial rate of absorption of CO_2 *RA* as a function of the equilibrium CO_2-loading $\tilde{X}_{CO_2}$ as determined from bubble cell experiments at 40 °C and a partial pressure of CO_2 of $p_{CO_2} = 140$ mbar, respectively. The mass fraction of amine in the unloaded solvent was $\tilde{w}^0_{\text{EvA}} = 0.05$ g/g in the experiments. This low mass fraction of amine in the unloaded solvent reduce the influence of the viscosity and surface tension on the initial rate of absorption [33] and additionally reduces the occurrence of solid precipitation. The data is divided into the same three groups as in the previous section: EvAs that contain oxygen-atoms, EvAs that do not contain

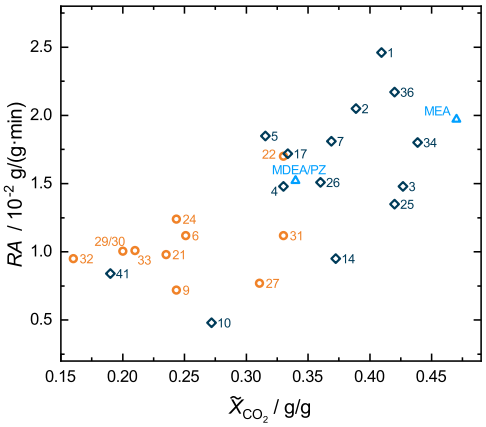

Figure 4: Initial rate of absorption of CO_2 as a function of the equilibrium CO_2-loading at 40 °C for aqueous solutions of amines with $\tilde{w}^0_{\text{amine}} = 0.05$ g/g at a partial pressure of CO_2 of $p_{CO_2} = 140$ mbar. Experimental results from bubble cell experiments of the present work. Numbers indicate the EvA-number. ○: EvAs that contain oxygen-atoms, ◇: EvAs that do not contain oxygen-atoms, △: references.

oxygen-atoms, and the references MEA and MDEA/PZ. The corresponding experimental numerical data are given in the Appendix.

A general trend of increasing RA with increasing $\tilde{X}_{CO_2}$ is observed (cf. Figure 4). $\tilde{X}_{CO_2}$ can be seen as the driving force for the absorption, and therefore strongly influences the initial rate of absorption. This explains the importance of high equilibrium CO_2-loadings $\tilde{X}_{CO_2}$ for reaching high rates of absorption RA. As discussed above, EvAs that do not contain oxygen-atoms show higher $\tilde{X}_{CO_2}$ than those that contain oxygen-atoms. Consequently, most of the EvAs that do not contain oxygen-atoms also show higher RA than those that contain oxygen-atoms.

EvA01, EvA02, and EvA36 show the highest RA in this comparison. It is remarkable that they even surpass the RA of MEA, although MEA is known to have high rate of absorption compared to many other amines [30, 32, 15, 40, 17, 46, 45]. As MEA has the highest $\tilde{X}_{CO_2}$, it is likely that EvA01, EvA36, and EvA02 have higher rates of reaction in the liquid phase than MEA. Other interesting candidates with high RA are EvA05, EvA07, EvA17, EvA22, and EvA34, which show similar RA as MEA and surpass that of MDEA/PZ. From these EvAs only EvA22 contains an oxygen-atom.

3.6. CO_2-solubility isotherms

Figure 5 shows the results of the head space gas chromatography measurements, in which the CO_2-solubility isotherms of aqueous solutions of amines with a mass fraction of amine in the unloaded solvent of $\tilde{w}^0_{\text{amine}} = 0.4$ g/g at 40 °C and 100 °C were determined. In Figure 5, the measured equilibrium partial pressure of CO_2 p_{CO_2} is plotted as a function

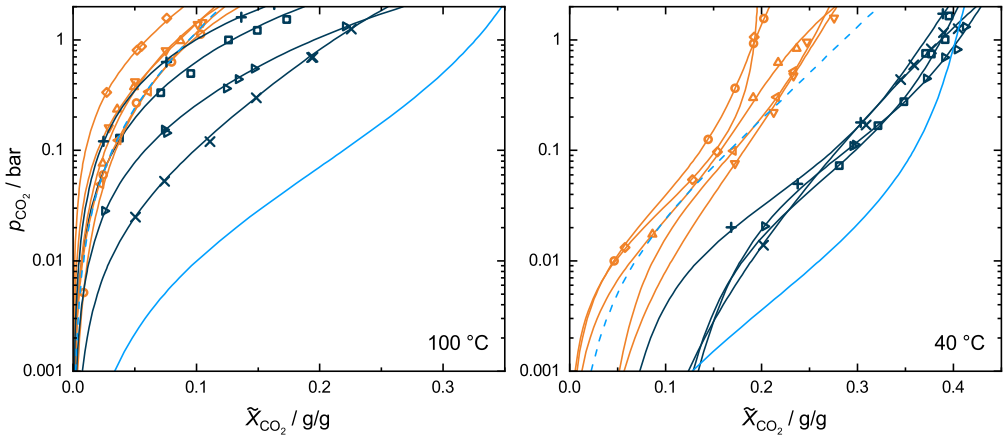

Figure 5: CO_2-solubility isotherms for aqueous solutions of amines with $\tilde{w}^0_{\text{amine}} = 0.4$ g/g. Left: 100 °C, right: 40 °C. Symbols: Experimental results from head space gas chromatography experiments of this work. Lines: SolSOFT equation fits. Orange: EvAs that contain oxygen-atoms, grey: EvAs that do not contain oxygen-atoms, blue: references. □ EvA03, ▽ EvA06, ◇ EvA09, ◁ EvA21, △ EvA24, + EvA25, ○ EvA29/30, ▷ EvA34, × EvA36, - - MDEA/PZ [64], — MEA [58].

of the CO_2-loading $\tilde{X}_{CO_2}$. The experimental results were correlated with the SolSOFT equation [1], which describes the data well. For comparison also results for MEA and MDEA/PZ are depicted, which were taken from the literature [58, 64]. Only aqueous solutions of EvAs that were classified as not solid precipitating (cf. Section 3.1) were studied with head space gas chromatography. The data is divided into the same three groups as in the previous section. The corresponding experimental numerical data are given in the Appendix. Also details on the correlation with the SolSOFT equation are given in the Appendix.

At 40 °C, EvAs that do not contain oxygen-atoms show higher CO_2-solubility than EvAs that contain oxygen-atoms. This is in accordance with the results of the equilibrium CO_2-loading from bubble cell experiments with lower mass fraction of amine in the unloaded solvent (cf. Section 3.4). The reference MEA shows the highest CO_2-solubility at 40 °C. The CO_2-solubility in MDEA/PZ is within the range of the EvAs that contain oxygen-atoms.

Also at 100 °C, most of the EvAs that do not contain oxygen-atoms show higher CO_2-solubility than the EvAs that contain oxygen-atoms. Exceptions are EvA25, and partially also EvA03. The remarkable low CO_2-solubility in EvA03 and EvA25 at 100 °C differs from the findings from bubble cell experiments, where the CO_2-solubility in EvA25 and EvA03 at 100 °C is higher than that in all EvAs that contain oxygen-atoms (cf. Figure 3). These differences result from the differences in the mass fraction of EvA in the unloaded solvent, which was $\tilde{w}^0_{\text{EvA}} = 0.4$ g/g here, whereas it was only $\tilde{w}^0_{\text{EvA}} = 0.05$ g/g in the

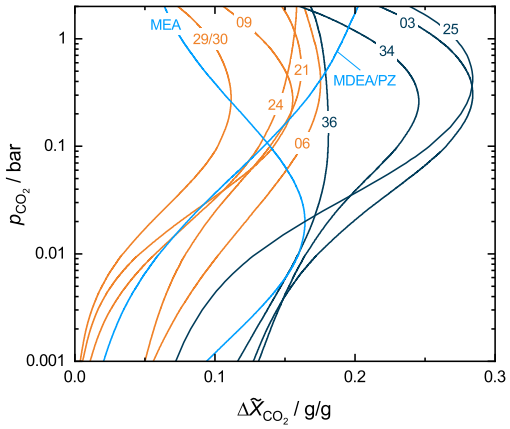

Figure 6: Differences between the CO_2-solubility isotherms at 40 °C and 100 °C (cf. Figure 5) for aqueous solutions of amines with $\tilde{w}^0_{\text{amine}} = 0.4$ g/g, calculated from SolSOFT fits. Orange: EvAs that contain oxygen-atoms, grey: EvAs that do not contain oxygen-atoms, blue: references. Numbers indicate the EvA-number.

bubble cell experiments. Of all studied amines, MEA shows the highest CO_2-solubility at 100 °C. The CO_2-solubility in MDEA/PZ is within the range of the CO_2-solubility in the EvAs that contain oxygen-atoms, EvA25, and EvA03.

Figure 6 shows the differences between the CO_2-solubility at 40 °C and 100 °C $\Delta\tilde{X}_{CO_2}$ for a given partial pressure of CO_2 p_{CO_2}. The displayed curves are calculated from the differences of the SolSOFT fits shown in Figure 5. The differences between the CO_2-solubility at 40 °C and 100 °C is a particularly important parameter for the absorption/desorption process and depends strongly on the partial pressure of CO_2. The results for $\Delta\tilde{X}_{CO_2}$ of the different amines differ strongly, however, most of the curves in Figure 6 show a distinct bulge. For MEA this bulge is at lower partial pressure of CO_2 than for the EvAs. For EvA24, EvA36, and MDEA/PZ, only a faint bulge is observed.

The results for $\Delta\tilde{X}_{CO_2}$ for the different amines follow the same trend that was observed for the equilibrium CO_2-loadings, cf. Section 3.4: EvAs that do not contain oxygen-atoms show larger $\Delta\tilde{X}_{CO_2}$ than EvAs that contain oxygen-atoms. MEA shows large $\Delta\tilde{X}_{CO_2}$ only in the lower partial pressure range, MDEA/PZ only in the upper partial pressure range. The $\Delta\tilde{X}_{CO_2}$ of the reference amines are surpassed by several of the EvAs. EvA03 shows the largest $\Delta\tilde{X}_{CO_2}$. This holds for the entire range of partial pressure of CO_2. EvA25 and EvA34 have similarly large $\Delta\tilde{X}_{CO_2}$, which are, however, slightly smaller than those of EvA03, either in the lower partial pressure range (EvA25) or upper partial pressure range (EvA34). EvA36 and EvA06 also have large $\Delta\tilde{X}_{CO_2}$ compared to most of the other amines.

3.7. NoVa short-cut method

The SolSOFT fits of the CO_2-solubility isotherms from Section 3.6 were used as input for a short-cut method for assessing the performance of the solvents in absorption/desorption processes. The method that was applied for this purpose is called NoVa [1] and is an improved version of the method of Notz et al.,which is known to give good results for amine based solvents [65, 66]. The method yields estimates for the specific energy demand and recirculation rate for a given CO_2-removal task. It is based on an equilibrium stage model in which it is assumed that both the absorber and the desorber have infinite separation capacity. It is known that the method is useful for the ranking of solvents, while the absolute numbers for a given solvent should not be over-interpreted [67], and the same applies for NoVa. The NoVa method is described in detail in [1], such that we focus on its application for assessing the EvAs here.

Two separation tasks were considered as scenarios for applying the NoVa method in this work. The first scenario is inspired by natural gas purification and labeled NG here. The second scenario is inspired by synthesis gas purification and labeled SG here. The values of the input parameters for the two scenarios were selected based on averaged values from literature [6, 8, 68] and are given in Table 7. They can be divided into three sets of input parameters. The first set contains specifications that characterize the purification scenario: the partial pressure of CO_2 at the inlet $p^{\mathrm{A,in}}_{\mathrm{CO_2}}$ and outlet $p^{\mathrm{A,out}}_{\mathrm{CO_2}}$ of the absorber, the pressure in the absorber p^{A}, and the average molar mass of the gas that is treated M_{gas}. Here, different values for the partial pressure of CO_2 at the inlet and outlet of the absorber were chosen to specify the removal tasks of the two scenarios. The removal rate of the scenario NG is 99.5 %. The removal rate of the scenario SG is 99.97 %.

The second set of input parameters are process parameters that specify the general framework of the absorption/desorption process: the pressure in the desorber p^{D}, the temperature of the CO_2-loaded aqueous solution at the desorber inlet $t^{\mathrm{D,rich}}$, the temperature inside the desorber $t^{\mathrm{D,lean}}$, and the temperature of the desorber condenser reflux $t^{\mathrm{D,cond}}$. The same process parameters were used in both scenarios. It follows from these choices that the heat recovery between the lean solution and the CO_2-loaded solution is assumed to be equal for all solvents in both scenarios.

The third set of input parameters are solvent parameters that characterize the physicochemical properties of the solvent: the liquid specific heat capacity of H_2O $c_{p,\mathrm{H_2O}}$ and of the solvent $c_{p,\mathrm{SOL}}$, the mass fraction of amine in the unloaded solvent $\tilde{w}^{0}_{\mathrm{amine}}$, the enthalpy of evaporation of H_2O $\Delta h^{\mathrm{vap}}_{\mathrm{H_2O}}$, the enthalpy of absorption of CO_2 $\Delta h^{\mathrm{abs}}_{\mathrm{CO_2}}$ in the solvent, and the solubility of CO_2 in the solvent at absorber $\tilde{\alpha}^{\mathrm{A}}_{\mathrm{CO_2}}(p_{\mathrm{CO_2}})$ and

desorber $\tilde{\alpha}^{\mathrm{D}}_{\mathrm{CO_2}}(p_{\mathrm{CO_2}})$ conditions, for which the SolSOFT isotherms at 40 ℃ and 100 ℃ from Section 3.6 were used here.

The enthalpy of absorption of CO_2 $\Delta h^{\mathrm{abs}}_{\mathrm{CO_2}}$ was not measured in this work. A workaround to estimate the enthalpy of absorption of CO_2 is to use a Gibbs-Helmholtz equation [69] with a temperature-dependent fit of the measured CO_2-solubility data, e.g. the temperature dependent version of the SolSOFT equation [1]. This workaround was tested but turned out to only provide strongly scattering results for $\Delta h^{\mathrm{abs}}_{\mathrm{CO_2}}$ as only two isotherms were measured. It was therefore assumed that $\Delta h^{\mathrm{abs}}_{\mathrm{CO_2}}$ is equal for all solvents. The chosen value of $\Delta h^{\mathrm{abs}}_{\mathrm{CO_2}}$ = -2 $\mathrm{kJ/g_{CO_2}}$ represents a crude approximation of the enthalpy of absorption of CO_2 that is reported in literature for aqueous solutions of MEA (-2 kJ/g ≥ $\Delta h^{\mathrm{abs}}_{\mathrm{CO_2}}$ ≥ -2.5 kJ/g [70, 58, 68, 8]) and MDEA/PZ (-1.6 kJ/g ≥ $\Delta h^{\mathrm{abs}}_{\mathrm{CO_2}}$ ≥ -2.2 kJ/g [68, 71]). Using the Gibbs-Helmholtz approach did not improve the accuracy of the values.

For a given ratio of the lean solvent mass flow to the rich gas mass flow L/G, the NoVa method yields the energy demand for the removal of one ton of CO_2 $q_{\mathrm{CO_2}}$. Hence, based on the results from NoVa, for all solvents, curves can be determined that show the energy demand $q_{\mathrm{CO_2}}$ as a function of the L/G ratio for the two scenarios. These curves are shown in the upper row diagrams of Figure 7 and are divided into the same three types of amines as in the previous sections. A detailed discussion and explanation of the basic structure of the U-shaped curves has been given in a previous work of our group [1]. The minimum of each curve is marked with an asterisk in Figure 7. It is the design point with the minimal energy demand $q^{\mathrm{opt}}_{\mathrm{CO_2}}$ and the optimal L/G. The minimal energy demand for each solvent is shown in the lower row diagrams of Figure 7. It consists of three contributions: the energy demand for the desorption of CO_2, the energy demand for solvent heating, and the energy demand for the production of stripping steam. The contribution for the desorption of CO_2 is the same for all solvents as the same amount of CO_2 is desorbed and the same enthalpy of desorption was used for all solvents (cf. Table 7). The energy demand for solvent heating and for the production of the stripping steam, as a result of the differences in their CO_2-solubility isotherms, however vary between the solvents. Therefore, the following discussion of the results of the NoVa method focuses only on these two energy contributions.

The higher amount of CO_2 in the scenario NG leads to higher L/G ratios, compared to the scenario SG. In general, the EvAs that do not contain oxygen-atoms show lower L/G ratios in the optimal operation point than EvAs that contain oxygen-atoms. This comes from the larger difference between the equilibrium CO_2-loadings at 40 ℃ and 100 ℃ of EvAs that do not contain oxygen-atoms (cf. Figure 6). Lower L/G ratios lead to

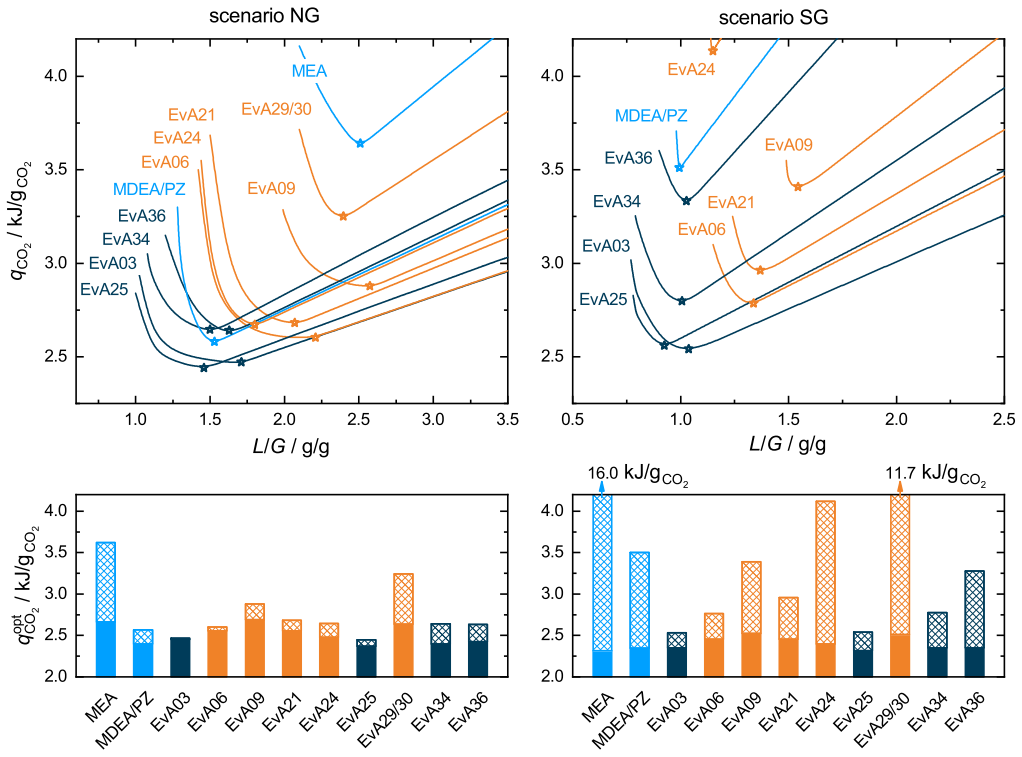

Figure 7: Results from the NoVa short-cut method for the scenario NG (left column) and SG (right column). Upper row: estimated energy demand as a function of the liquid-to-gas ratio in the absorber. ☆: optimal operation point. Lower row: Energy contribution in the optimal operation point. ■: solvent heating, ⊠: stripping steam production. The intercept of 2 kJ/g_{CO_2} equals the assumed enthalpy of desorption (see text). Orange: EvAs that contain oxygen-atoms, grey: EvAs that do not contain oxygen-atoms, blue: references.

lower energy demand for solvent heating. This is particularly relevant for purification tasks, where the amount of CO_2 is high and the purification requirement is low.

The higher purification requirement in the scenario SG leads to a higher energy demand for the production of stripping steam compared to the scenario NG. This amplifies the differences between the solvents. Low CO_2-solubility at 100 ℃ (cf. Figure 5) and a large difference between the CO_2-solubility isotherms at 40 ℃ and 100 ℃ (cf. Figure 6) are favorable as they reduce the energy demand for the production of stripping steam. A comparison of the results of EvA25 and EvA34 as well as of EvA06 and EvA36 indicates that a low CO_2-solubility at 100 ℃ has stronger impact on the energy demand for the production of stripping steam than the difference between the CO_2-solubility isotherms at 40 ℃ and 100 ℃. This is particularly relevant if the purification requirement is high.

All EvAs that were studied here show a significantly lower estimated energy demand than the reference MEA in both scenarios. This result would probably remain valid if measured enthalpies of absorption of CO_2 for each solvent had been used. The difference

between the estimated energy demand of the EvAs compared to that of the reference MDEA/PZ are less significant. Here, the applied assumption of equal enthalpies of absorption of CO_2 for all solvents limits the validity of the ranking. Nevertheless, most of the EvAs perform well. Especially EvA03 and EvA25 show favorable shapes of their CO_2-solubility isotherms which results in the lowest estimated energy demand in both scenarios in the present ranking. In the scenario SG, the estimated energy reduction of EvA03 and EvA25 is about 25 % compared to MDEA/PZ. Besides EvA03 and EvA25, also EvA06, EvA34 and EvA21 are interesting candidates.

Table 7: Input parameters that were used in the NoVa short-cut method for the natural gas (NG) and synthesis gas (SG) scenarios. The CO_2-solubility was described with the SolSOFT fits of the CO_2-solubility isotherms. The symbols are explained in the text.

parameter	scenario NG / SG
specifying parameters	
$p^{\mathrm{A,in}}_{\mathrm{CO_2}}$ / bar	2.0 / 1.5
$p^{\mathrm{A,out}}_{\mathrm{CO_2}}$ / bar	0.01 / 0.0005
p^{A} / bar	35
M_{gas} / g/mol	16
process parameters	
p^{D} / bar	2
$t^{\mathrm{D,rich}}$ / °C	90
$t^{\mathrm{D,lean}}$ / °C	100
$t^{\mathrm{D,cond}}$ / °C	20
solvent parameters	
$c_{p,\mathrm{H_2O}}$ / kJ/(kg · K)	4.20
$c_{p,\mathrm{SOL}}$ / kJ/(kg · K)	4.05
$\tilde{w}^{0}_{\mathrm{amine}}$ / g/g	0.4
$\Delta h^{\mathrm{vap}}_{\mathrm{H_2O}}$ / kJ/g	2.21
$\Delta h^{\mathrm{abs}}_{\mathrm{CO_2}}$ / kJ/g	-2
$\tilde{\alpha}^{\mathrm{A}}_{\mathrm{CO_2}}(p_{\mathrm{CO_2}})$ / g/g $\tilde{\alpha}^{\mathrm{D}}_{\mathrm{CO_2}}(p_{\mathrm{CO_2}})$ / g/g	cf. Table A10

3.8. Summary of results

Some of the EvAs that were synthesized turned out to be only poorly soluble in water and were not investigated further. No problems with foaming occurred in the

tests with the EvAs in aqueous solution. For two of the EvAs, the tendency for foaming was similar to that of MEA and MDEA/PZ. For all others it was distinctly lower. The dynamic viscosities of the studied aqueous solutions of EvAs are higher than those of corresponding solutions of MEA and MDEA/PZ. This is undesired, but there are many EvAs with moderate viscosities that are acceptable for applications.

In several of the studied aqueous solutions of EvAs, a liquid-liquid phase separation occurs at elevated temperatures. The demixing temperatures vary strongly, depending on the substituent of the EvA. As expected, polar groups increase the demixing temperature. There is an ongoing discussion whether such a liquid-liquid phase separation can be used in an advantageous way in CO_2-absorption processes [72, 73, 74, 75, 76, 77, 78, 79, 80]. EvA solutions can be interesting test systems for studying this question in detail. Such a study is in progress for EvA25 in our laboratory.

After loading with CO_2, solid precipitation was observed in some of the studied aqueous solutions of EvA. This process can be very slow and it may take days until the solid forms. The probability of solid precipitation increases with increasing mass fraction of amine in the unloaded solvent. Solid precipitation is generally undesired. But, similar to the liquid-liquid phase separation, it has been argued that also solid precipitation could be beneficially used in CO_2-absorption processes [81, 82, 83]. The basic idea is in both cases that the occurrence of a new phase leads to a split of the CO_2 between these phases and the hope is that a process can be designed in such a way as to make use of this. EvAs could also be interesting candidates for studying CO_2-absorption processes with solid precipitation.

The solubility of CO_2 in the aqueous solutions of amines is of outstanding importance for the capture process and was studied both with a bubble cell and by head space gas chromatography in the present work. Two mass fractions of amine in the unloaded solvent were investigated ($\tilde{w}^0_{\mathrm{EvA}} = 0.05$ g/g and $\tilde{w}^0_{\mathrm{EvA}} = 0.4$ g/g). Generally, aqueous solutions of EvAs that do not contain oxygen-atoms showed higher equilibrium CO_2-loadings than the ones that contain oxygen-atoms. This holds both for the results at 40 °C and 100 °C (absorber and desorber conditions). The EvAs that do not contain oxygen-atoms have also a larger difference between the equilibrium CO_2-loadings at absorption and desorption conditions. Also the measured pK-values follow this trend: they are generally higher for EvAs that do not contain oxygen-atoms.

Furthermore, rates of absorption of CO_2 were studied in bubble cell experiments. A low mass fraction of amine in the unloaded solvent was used in these studies to minimize the influence of the viscosity and surface tension. The initial rates of absorption of CO_2 in the aqueous solutions of EvAs that do not contain oxygen-atoms are generally higher

than those for EvAs that contain oxygen-atoms. This is partially related to the fact that the EvAs that do not contain oxygen-atoms also have a higher equilibrium CO_2-loading and that there is a general trend that high equilibrium CO_2-loadings lead to high rates of absorption of CO_2 as the potential difference that drives the absorption of CO_2 is higher.

The CO_2-solubility isotherms that were measured in the present work, were correlated empirically with the SolSOFT equation, which was introduced recently by our group [1]. This information enables the application of a short-cut method for assessing solvents for CO_2-absorption. The basic method for this purpose was developed some years ago by our group and is known to give good results for ranking solvents [67]. The method has recently been overhauled and the new version is called NoVa [1]. One of the advantages of NoVa is that it gives deep insight on the limitations of the absorption/desorption process. As its predecessor, NoVa yields a curve that relates the specific regeneration energy that is required for a given purification task to the ratio of the solvent flow rate and the feed gas flow rate. From that curve, the optimal liquid-to-gas ratio for the solvent and the minimal regeneration energy demand can be determined. The NoVa method was applied to all EvAs for which CO_2-solubility isotherms were measured, as well as to the references MEA and MDEA/PZ. The purification tasks that were considered here are natural gas and synthesis gas cleaning. As expected, MEA is not an attractive solvent for these applications, in which MDEA/PZ is often used. Several of the EvAs outperform MDEA/PZ in this assessment. This shows the potential of the EvAs.

4. Conclusion

A new class of amines for the CO_2-absorption from process gases was investigated in a broad experimental study. The new amines are derivates of triacetoneamine and called EvAs here. They have the same basic ring structure but different substituents. 26 EvAs were synthesized for the present work and studied in a consistent manner. MEA and MDEA/PZ were included in the study as references and treated the same way as the EvAs.

Overall, the aqueous solutions of EvA02, EvA03, EvA25, and EvA34 emerge as the most promising candidates from the present study. EvA34 has already been studied comprehensively in a previous work of our group [57]. The results from that study are in good agreement with those of the present work, revealing aqueous solutions of EvA34 as highly interesting solvents for the CO_2-absorption from process gases. EvA02 was also studied in a previous work of our group [26]. However, solid precipitation occurs for EvA02 even at low mass fraction of the amine, which makes the solvent difficult to apply in conventional absorption/desorption processes. EvA25 is highly interesting due to the

good performance and the liquid-liquid demixing. EvA03 is an excellent candidate as it gave good results throughout this screening.

This study provides also a broad basis for establishing structure-property-relationships that relate the molecule structure of amines to properties of the aqueous solution of the amines which are relevant for the CO_2-absorption. Only some aspects of this have been discussed in the present work. Some more information on this topic is available in a preliminary report [27]. A comprehensive report, that will also include systematic studies of the chemical reactions in CO_2-loaded aqueous solutions of EvAs, is presently in preparation.

5. Acknowledgement

We gratefully acknowledge the financial support of this work by the Federal Ministry of Economic Affairs and Energy of the Federal Republic of Germany (grant no. 03ET1098) and by Evonik and thyssenkrupp.

6. Appendix

6.1. Experimental numerical data

The experimental numerical data from bubble cell experiments of this work are given in Table A8. A preliminary report of the results has been given in a conference paper [27]. The data that were presented in that paper and the data from the present work are not identical, as the primary IR data was reevaluated. It is recommended to use the data reported in the present work. The trends and basic findings of both publications match perfectly. The experimental numerical data from head space gas chromatography experiments of this work are given in Table A9.

Table A8: Initial rate of absorption of CO_2 and equilibrium CO_2-loading from bubble cell experiments of this work with $\tilde{w}^0_{\text{amine}} = 0.05$ g/g and $p_{CO_2} = 140$ mbar.

	RA	$\tilde{X}_{CO_2}$	
	10^{-2} g/(g·min)	g/g	
t / ℃	40	40	100
MEA	1.97	0.47	0.27
MDEA/PZ	1.52	0.34	0.11
EvA01	2.46	0.41	0.27

continued on next page

Table A8: continued from previous page

	RA	$\tilde{X}_{CO_2}$	
	10^{-2} g/(g·min)	g/g	
t / ℃	40	40	100
EvA02	2.05	0.39	0.16
EvA03	1.48	0.43	0.20
EvA04	1.48	0.33	0.18
EvA05	1.85	0.32	0.17
EvA06	1.12	0.25	0.14
EvA07	1.81	0.37	0.15
EvA09	0.72	0.24	0.12
EvA10	0.48	0.27	0.12
EvA14	0.95	0.37	0.16
EvA17	1.72	0.33	0.17
EvA21	0.98	0.24	0.13
EvA22	1.70	0.33	0.16
EvA24	1.24	0.24	0.12
EvA25	1.35	0.42	0.20
EvA26	1.51	0.36	0.15
EvA27	0.77	0.31	0.15
EvA29/30	1.00	0.20	0.11
EvA31	1.25	0.33	0.17
EvA32	0.95	0.16	0.09
EvA33	1.01	0.21	0.09
EvA34	1.80	0.44	0.21
EvA36	2.17	0.42	0.24
EvA41	0.84	0.19	0.08

continued on next page

Table A8: continued from previous page

	RA	$\tilde{X}_{CO_2}$	
	10^{-2} g/(g·min)	g/g	
t / ℃	40	40	100

$\tilde{w}^0_{amine}$: mass fraction of amine in the unloaded solvent with the relative expanded uncertainty $u_r(\tilde{w}^0_{amine}) = 0.001$ (0.99 level of confidence), p_{CO_2}: partial pressure of CO_2 with the standard uncertainty $u(p_{CO_2}) = 5$ mbar, RA: initial rate of absorption of CO_2 with the relative standard uncertainty $u_r(RA) = 0.05$, $\tilde{X}_{CO_2}$: equilibrium CO_2-loading with the relative standard uncertainty $u_r(\tilde{X}_{CO_2}) = 0.05$, t: temperature with the expanded uncertainty $U(t) = 1$ ℃ (0.99 level of confidence).

Table A9: CO_2-solubility from head space gas chromatography experiments of this work with with $\tilde{w}^0_{EvA} = 0.4$ g/g.

t / ℃	40		100		40		100	
	$\tilde{X}_{CO_2}$	p_{CO_2}	$\tilde{X}_{CO_2}$	p_{CO_2}	$\tilde{X}_{CO_2}$	p_{CO_2}	$\tilde{X}_{CO_2}$	p_{CO_2}
	g/g	bar	g/g	bar	g/g	bar	g/g	bar
	EvA03				EvA06			
	0.281	0.073	0.038	0.129	0.172	0.076	0.029	0.161
	0.321	0.167	0.071	0.332	0.213	0.221	0.050	0.420
	0.348	0.275	0.095	0.495	0.233	0.474	0.075	0.804
	0.371	0.754	0.126	0.997	0.247	0.960	0.101	1.382
	0.377	0.746	0.149	1.225	0.276	1.586	0.105	1.447
	0.391	1.005	0.173	1.531				
	0.395	1.646						
	EvA09				EvA21			
	0.058	0.013	0.027	0.334	0.171	0.099	0.022	0.049
	0.128	0.054	0.052	0.807	0.216	0.304	0.037	0.123
	0.154	0.097	0.056	0.876	0.234	0.521	0.061	0.339
	0.192	1.059	0.076	1.569				
	EvA24				EvA25			
	0.086	0.017	0.024	0.076	0.168	0.020	0.025	0.121
	0.191	0.299	0.036	0.236	0.238	0.050	0.076	0.632

continued on next page

Table A9: continued from previous page

t / ℃	40		100		40		100	
	$\tilde{X}_{CO_2}$ g/g	p_{CO_2} bar	$\tilde{X}_{CO_2}$ g/g	p_{CO_2} bar	$\tilde{X}_{CO_2}$ g/g	p_{CO_2} bar	$\tilde{X}_{CO_2}$ g/g	p_{CO_2} bar
	0.217	0.621	0.049	0.375	0.303	0.179	0.136	1.605
	0.237	0.836	0.087	0.982	0.389	1.728	0.163	2.103
	EvA29/30				EvA34			
	0.046	0.010	0.009	0.005	0.203	0.021	0.025	0.028
	0.144	0.126	0.024	0.060	0.295	0.109	0.074	0.154
	0.172	0.365	0.051	0.269	0.298	0.113	0.076	0.144
	0.192	0.926	0.080	0.632	0.372	0.445	0.124	0.363
	0.202	1.566	0.103	1.130	0.391	0.694	0.134	0.439
					0.404	0.817	0.147	0.548
					0.412	1.312	0.221	1.326
	EvA36							
	0.202	0.014	0.050	0.025				
	0.309	0.170	0.074	0.053				
	0.345	0.438	0.111	0.120				
	0.359	0.593	0.149	0.300				
	0.377	0.831	0.193	0.694				
	0.390	1.167	0.194	0.699				
	0.405	1.265	0.226	1.251				

$\tilde{w}^0_{EvA}$: mass fraction of amine in the unloaded solvent with the relative expanded uncertainty $u_r(\tilde{w}^0_{EvA}) = 0.001$ (0.99 level of confidence), t: temperature with the expanded uncertainty $U(t) = 0.1$ ℃ (0.99 level of confidence), $\tilde{X}_{CO_2}$: equilibrium CO_2-loading with the relative expanded uncertainty $U_r(\tilde{X}_{CO_2}) = 0.01$ (0.99 level of confidence), p_{CO_2}: partial pressure of CO_2 with the relative standard uncertainty $u_r(p_{CO_2}) = 0.08$.

6.2. SolSOFT equation and parameters

The SolSOFT equation, which was used in the present work to describe gas solubility data, is given in equation (1). For more information, see [1, 26].

$$\tilde{X}_{\mathrm{CO_2}} = \frac{M_{\mathrm{CO_2}}}{M_{\mathrm{amine}}} \cdot \left[\left(\frac{p_{\mathrm{CO_2}}}{K_p} \right)^m + n \cdot \frac{\left(\frac{p_{\mathrm{CO_2}}}{K_c} \right)^n}{1 + \left(\frac{p_{\mathrm{CO_2}}}{K_c} \right)^n} \right] \tag{1}$$

In the equation $\tilde{X}_{\mathrm{CO_2}}$ is the equilibrium CO_2-loading, $p_{\mathrm{CO_2}}$ is the partial pressure of CO_2, and $M_{\mathrm{CO_2}}$ and M_{amine} are the molar masses of CO_2 and the amine, respectively. K_p, K_c, m and n are parameters. They were determined from a fit to the CO_2-solubility data from the head space gas chromatography experiments (cf. Table A9). The resulting parameters are given in Table A10. The parameters for MEA and MDEA/PZ were determined from a fit to simulation data (MEA: [58] and MDEA/PZ: [64]). The mass fraction of amine in the unloaded solvent was $\tilde{w}^0_{\mathrm{amine}} = 0.4$ g/g for all solvents.

Table A10: Parameters for the SolSOFT equation (Equation 1) for describing the CO_2-solubility in the studied aqueous solutions of amines.

solvent	t / ℃	K_p	K_c	m	n
MEA	40	450	0.004	0.8	0.58
	100	1500	0.07	0.92	0.56
MDEA/PZ	40	71	0.082	0.35	0.62
	100	450	2.1	0.99	0.62
EvA03	40	0.1	0.052	0.082	0.97
	100	4	1.2	0.7	0.7
EvA06	40	9.3	0.032	0.17	0.63
	100	80	1.15	0.9	0.85
EvA09	40	184	0.031	2.74	1.02
	100	60	2.4	0.9	0.9
EvA21	40	2.4	0.07	0.14	0.92
	100	10	0.45	0.7	0.7
EvA24	40	3	0.019	0.45	0.96
	100	7	0.8	0.8	0.62
EvA25	40	0.3	0.035	0.15	1.1
	100	2.9	8	0.7	0.6
EvA29/30	40	38	0.031	0.44	0.96
	100	6	0.6	0.7	0.5
EvA34	40	0.003	0.094	0.095	1.09
	100	1.5	0.4	0.6	0.8

continued on next page

Table A10: continued from previous page

solvent	t / ℃	K_p	K_c	m	n
EvA36	40	0.05	0.025	0.15	0.5
	100	5	0.12	0.47	0.75

t: temperature. K_p; K_c; m; n: Parameters for the SolSOFT equation (cf. Equation (1))

References

[1] D. Vasiliu, E. Kessler, E. von Harbou, H. Hasse, Short-cut method for assessing solvents for gas cleaning by reactive absorption, Chemical Engineering Research and Design 153 (2020) 757–767. doi:10.1016/j.cherd.2019.10.015.

[2] T. Kuramochi, A. Ramírez, W. Turkenburg, A. Faaij, Comparative assessment of co2 capture technologies for carbon-intensive industrial processes, Progress in Energy and Combustion Science 38 (2012) 87–112. doi:10.1016/j.pecs.2011.05.001.

[3] T. E. Rufford, S. Smart, G. C. Y. Watson, B. F. Graham, J. Boxall, J. C. D. d. Costa, E. F. May, The removal of co2 and n2 from natural gas: A review of conventional and emerging process technologies, Journal of Petroleum Science and Engineering 94-95 (2012) 123–154. doi:10.1016/j.petrol.2012.06.016.

[4] M. K. Mondal, H. K. Balsora, P. Varshney, Progress and trends in co2 capture/separation technologies: A review, Energy 46 (2012) 431–441. doi:10.1016/j.energy.2012.08.006.

[5] B. Li, Y. Duan, D. Luebke, B. Morreale, Advances in co2 capture technology: A patent review, Applied Energy 102 (2013) 1439–1447. doi:10.1016/j.apenergy.2012.09.009.

[6] B. Metz, O. Davidson, H. de Coninck, M. Loos, L. Meyer, IPCC special report on carbon dioxide capture and storage, IPCC, Genf, 2005.

[7] International Energy Agency, Technology Roadmap Carbon Capture and Storage: Carbon Capture and Storage, IEA Technology Roadmaps, OECD Publishing, Paris, 2009.

[8] A. L. Kohl, R. Nielsen, Gas purification, 5th Edition, Gulf Publishing Company, Houston, 1997.

[9] Hydrocarbon Processing Industry, 2012 Gas Processes Handbook, Gulf Publishing Company, Houston, 2012.

[10] Ö. Yildirim, A. A. Kiss, N. Hüser, K. Leßmann, E. Y. Kenig, Reactive absorption in chemical process industry: A review on current activities, Chemical Engineering Journal 213 (2012) 371–391. doi:10.1016/j.cej.2012.09.121.

[11] C. M. Quintella, S. A. Hatimondi, A. P. S. Musse, S. F. Miyazaki, G. S. Cerqueira, A. d. A. Moreira, Co2 capture technologies: An overview with technology assessment based on patents and articles, Energy Procedia 4 (2011) 2050–2057. doi:10.1016/j.egypro.2011.02.087.

[12] Z. Liang, W. Rongwong, H. Liu, K. Fu, H. Gao, F. Cao, R. Zhang, T. Sema, A. Henni, K. Sumon, D. Nath, D. Gelowitz, W. Srisang, C. Saiwan, A. Benamor, M. Al-Marri, H. Shi, T. Supap, C. Chan, Q. Zhou, M. Abu-Zahra, M. Wilson, W. Olson, R. Idem, P. Tontiwachwuthikul, Recent progress and new developments in post-combustion carbon-capture technology with amine based solvents, International Journal of Greenhouse Gas Control 40 (2015) 26–54. doi:10.1016/j.ijggc.2015.06.017.

[13] I. M. Bernhardsen, H. K. Knuutila, A review of potential amine solvents for co2 absorption process: Absorption capacity, cyclic capacity and pka, International Journal of Greenhouse Gas Control 61 (2017) 27–48. doi:10.1016/j.ijggc.2017.03.021.

[14] F. A. Chowdhury, H. Okabe, S. Shimizu, M. Onoda, Y. Fujioka, Development of novel tertiary amine absorbents for co2 capture, Energy Procedia 1 (2009) 1241–1248. doi:10.1016/j.egypro.2009.01.163.

[15] F. A. Chowdhury, H. Okabe, H. Yamada, M. Onoda, Y. Fujioka, Synthesis and selection of hindered new amine absorbents for co2 capture, Energy Procedia 4 (2011) 201–208. doi:10.1016/j.egypro.2011.01.042.

[16] F. A. Chowdhury, H. Yamada, T. Higashii, Y. Matsuzaki, S. Kazama, Synthesis and characterization of new absorbents for co2 capture, Energy Procedia 37 (2013) 265–272. doi:10.1016/j.egypro.2013.05.111.

[17] K. Goto, F. A. Chowdhury, H. Okabe, S. Shimizu, Y. Fujioka, Development of a low cost co2 capture system with a novel absorbent under the cocs project, Energy Procedia 4 (2011) 253–258. doi:10.1016/j.egypro.2011.01.049.

[18] K. Goto, H. Okabe, F. A. Chowdhury, S. Shimizu, Y. Fujioka, M. Onoda, Development of novel absorbents for co2 capture from blast furnace gas, International Journal of Greenhouse Gas Control 5 (2011) 1214–1219. doi:10.1016/j.ijggc.2011.06.006.

[19] W. Conway, Q. Yang, S. James, C.-C. Wei, M. Bown, P. Feron, G. Puxty, Designer amines for post combustion co2 capture processes, Energy Procedia 63 (2014) 1827–1834. doi:10.1016/j.egypro.2014.11.190.

[20] Q. Yang, G. Puxty, S. James, M. Bown, P. Feron, W. Conway, Toward intelligent co 2 capture solvent design through experimental solvent development and amine synthesis, Energy & Fuels 30 (2016) 7503–7510. doi:10.1021/acs.energyfuels.6b00875.

[21] R. J. Hook, An investigation of some sterically hindered amines as potential carbon dioxide scrubbing compounds, Industrial & Engineering Chemistry Research 36 (1997) 1779–1790. doi:10.1021/ie9605589.

[22] K. Maneeintr, R. O. Idem, P. Tontiwachwuthikul, A. G. H. Wee, Synthesis, solubilities, and cyclic capacities of amino alcohols for co2 capture from flue gas streams, Energy Procedia 1 (2009) 1327–1334. doi:10.1016/j.egypro.2009.01.174.

[23] S. Singto, T. Supap, R. Idem, P. Tontiwachwuthikul, S. Tantayanon, M. J. Al-Marri, A. Benamor, Synthesis of new amines for enhanced carbon dioxide (co2) capture performance: The effect of chemical structure on equilibrium solubility, cyclic capacity, kinetics of absorption and regeneration, and heats of absorption and regeneration, Separation and Purification Technology 167 (2016) 97–107. doi:10.1016/j.seppur.2016.05.002.

[24] J. Salazar, U. Diwekar, K. Joback, A. H. Berger, A. S. Bhown, Solvent selection for post-combustion co2 capture, Energy Procedia 37 (2013) 257–264. doi:10.1016/j.egypro.2013.05.110.

[25] T. Zarogiannis, A. I. Papadopoulos, P. Seferlis, Systematic selection of amine mixtures as post-combustion co2 capture solvent candidates, Journal of Cleaner Production 136 (2016) 159–175. doi:10.1016/j.jclepro.2016.04.110.

[26] D. Vasiliu, A. Yazdani, N. McCann, M. Irfan, R. Schneider, J. Rolker, G. Maurer, E. von Harbou, H. Hasse, Thermodynamic study of a complex system for carbon capture: Butyltriacetonediamine + water + carbon dioxide, Journal of Chemical & Engineering Data 61 (2016) 3814–3826. doi:10.1021/acs.jced.6b00451.

[27] E. Kessler, L. Ninni Schäfer, B. Willy, R. Schneider, M. Irfan, J. Rolker, E. von Harbou, H. Hasse, Structure-property relationships for new amines for reactive co2 absorption, Chemical Engineering Transactions 69 (2018) 109–114. doi:10.3303/CET1869019.

[28] A. Adeosun, Z. Abbas, M. R. Abu-Zahra, Screening and characterization of advanced amine based solvent systems for co2 post-combustion capture, Energy Procedia 37 (2013) 300–305. doi:10.1016/j.egypro.2013.05.115.

[29] U. E. Aronu, H. F. Svendsen, K. A. Hoff, Investigation of amine amino acid salts for carbon dioxide absorption, International Journal of Greenhouse Gas Control 4 (2010) 771–775. doi:10.1016/j.ijggc.2010.04.003.

[30] U. E. Aronu, K. A. Hoff, H. F. Svendsen, Co2 capture solvent selection by combined absorption–desorption analysis, Chemical Engineering Research and Design 89 (2011) 1197–1203. doi:10.1016/j.cherd.2011.01.007.

[31] U. E. Aronu, A. F. Ciftja, I. Kim, A. Hartono, Understanding precipitation in amino acid salt systems at process conditions, Energy Procedia 37 (2013) 233–240. doi:10.1016/j.egypro.2013.05.107.

[32] P. Brœder, H. F. Svendsen, Capacity and kinetics of solvents for post-combustion co2 capture, Energy Procedia 23 (2012) 45–54. doi:10.1016/j.egypro.2012.06.028.

[33] X. Chen, F. Closmann, G. T. Rochelle, Accurate screening of amines by the wetted wall column, Energy Procedia 4 (2011) 101–108. doi:10.1016/j.egypro.2011.01.029.

[34] X. Chen, G. T. Rochelle, Aqueous piperazine derivatives for co2 capture: Accurate screening by a wetted wall column, Chemical Engineering Research and Design 89 (2011) 1693–1710. doi:10.1016/j.cherd.2011.04.002.

[35] S. Y. Choi, S. C. Nam, Y. I. Yoon, K. T. Park, S.-J. Park, Carbon dioxide absorption into aqueous blends of methyldiethanolamine (mdea) and alkyl amines containing multiple amino groups, Industrial & Engineering Chemistry Research 53 (2014) 14451–14461. doi:10.1021/ie502434m.

[36] W. Conway, Y. Beyad, P. Feron, G. Richner, G. Puxty, Co2 absorption into aqueous amine blends containing benzylamine (bza), monoethanolamine (mea), and sterically hindered/tertiary amines, Energy Procedia 63 (2014) 1835–1841. doi:10.1016/j.egypro.2014.11.191.

[37] Y. Du, Y. Yuan, G. T. Rochelle, Capacity and absorption rate of tertiary and hindered amines blended with piperazine for co 2 capture, Chemical Engineering Science 155 (2016) 397–404. doi:10.1016/j.ces.2016.08.017.

[38] L. Dubois, D. Thomas, Postcombustion co2 capture by chemical absorption: Screening of aqueous amine(s)-based solvents, Energy Procedia 37 (2013) 1648–1657. doi:10.1016/j.egypro.2013.06.040.

[39] N. El Hadri, D. V. Quang, E. L. Goetheer, M. R. Abu Zahra, Aqueous amine solution characterization for post-combustion co 2 capture process, Applied Energy 185 (2017) 1433–1449. doi:10.1016/j.apenergy.2016.03.043.

[40] A. Hartono, S. J. Vevelstad, A. Ciftja, H. K. Knuutila, Screening of strong bicarbonate forming solvents for co 2 capture, International Journal of Greenhouse Gas Control 58 (2017) 201–211. doi:10.1016/j.ijggc.2016.12.018.

[41] Y. E. Kim, S. J. Moon, Y. I. Yoon, S. K. Jeong, K. T. Park, S. T. Bae, S. C. Nam, Heat of absorption and absorption capacity of co2 in aqueous solutions of amine containing multiple amino groups, Separation and Purification Technology 122 (2014) 112–118. doi:10.1016/j.seppur.2013.10.030.

[42] X. Luo, S. Liu, H. Gao, H. Liao, P. Tontiwachwuthikul, Z. Liang, An improved fast screening method for single and blended amine-based solvents for post-combustion co2 capture, Separation and Purification Technology 169 (2016) 279–288. doi:10.1016/j.seppur.2016.06.018.

[43] Y. Mergler, R. R.-v. Gurp, P. Brasser, M. d. Koning, E. Goetheer, Solvents for co2 capture. structure-activity relationships combined with vapour-liquid-equilibrium measurements, Energy Procedia 4 (2011) 259–266. doi:10.1016/j.egypro.2011.01.050.

[44] P. Muchan, C. Saiwan, J. Narku-Tetteh, R. Idem, T. Supap, P. Tontiwachwuthikul, Screening tests of aqueous alkanolamine solutions based on primary, secondary, and tertiary structure for blended aqueous amine solution selection in post combustion co 2 capture, Chemical Engineering Science 170 (2017) 574–582. doi:10.1016/j.ces.2017.02.031.

[45] P. Muchan, J. Narku-Tetteh, C. Saiwan, R. Idem, T. Supap, P. Tontiwachwuthikul, Effect of number of hydroxyl group in sterically hindered alkanolamine on co 2 capture activity, Energy Procedia 114 (2017) 1966–1972. doi:10.1016/j.egypro.2017.03.1328.

[46] G. Puxty, R. Rowland, A. Allport, Q. Yang, M. Bown, R. Burns, M. Maeder, M. Attalla, Carbon dioxide postcombustion capture: A novel screening study of the carbon dioxide absorption performance of 76 amines, Environmental Science & Technology 43 (2009) 6427–6433. doi:10.1021/es901376a.

[47] P. Singh, J. P. M. Niederer, G. F. Versteeg, Structure and activity relationships for amine based co2 absorbents—i, International Journal of Greenhouse Gas Control 1 (2007) 5–10. doi:10.1016/S1750-5836(07)00015-1.

[48] P. Singh, D. Brilman, M. Groeneveld, Solubility of co2 in aqueous solution of newly developed absorbents, Energy Procedia 1 (2009) 1257–1264. doi:10.1016/j.egypro.2009.01.165.

[49] P. Singh, J. P. M. Niederer, G. F. Versteeg, Structure and activity relationships for amine-based co2 absorbents-ii, Chemical Engineering Research and Design 87 (2009) 135–144. doi:10.1016/j.cherd.2008.07.014.

[50] P. Singh, D. W. F. Brilman, M. J. Groeneveld, Evaluation of co2 solubility in potential aqueous amine-based solvents at low co2 partial pressure, International Journal of Greenhouse Gas Control 5 (2011) 61–68. doi:10.1016/j.ijggc.2010.06.009.

[51] Z. Wang, M. Fang, Y. Pan, S. Yan, Z. Luo, Comparison and selection of amine-based absorbents in membrane vacuum regeneration process for co2 capture with low energy cost, Energy Procedia 37 (2013) 1085–1092. doi:10.1016/j.egypro.2013.05.205.

[52] Z. Wang, M. Fang, Y. Pan, S. Yan, Z. Luo, Amine-based absorbents selection for co2 membrane vacuum regeneration technology by combined absorption–desorption analysis, Chemical Engineering Science 93 (2013) 238–249. doi:10.1016/j.ces.2013.01.057.

[53] R. Zhang, Q. Yang, Z. Liang, G. Puxty, R. J. Mulder, J. E. Cosgriff, H. Yu, X. Yang, Y. Xue, Toward efficient co2 capture solvent design by analyzing the effect of chain lengths and amino types to the absorption capacity, bicarbonate/carbamate, and cyclic capacity, Energy & Fuels 31 (2017) 11099–11108. doi:10.1021/acs.energyfuels.7b01951.

[54] A. T. Zoghi, F. Feyzi, S. Zarrinpashneh, Experimental investigation on the effect of addition of amine activators to aqueous solutions of n-methyldiethanolamine on the rate of carbon dioxide absorption, International Journal of Greenhouse Gas Control 7 (2012) 12–19. doi:10.1016/j.ijggc.2011.12.001.

[55] S. G. Warren, P. Wyatt, Organic Synthesis: The Disconnection Approach, 2nd Edition, Wiley-Blackwell, Oxford, 2008.

[56] K. Minke, B. Willy, Us patent 20180009734r: An n-substituted triacetonediamine compound is produced by reacting 4-amino-2,2,6,6-tetramethylpiperidine or a derivative thereof with a carbonyl compound in a reductive amination (2018).

[57] E. Kessler, L. Ninni, T. Breug-Nissen, B. Willy, R. Schneider, M. Irfan, J. Rolker, E. von Harbou, H. Hasse, Physicochemical properties of the system n,n-dimethyldipropylene-diamino-triacetonediamine (eva34), water, and carbon dioxide for re-

active absorption, Journal of Chemical & Engineering Data 64 (2019) 2368–2379. doi:10.1021/acs.jced.8b01174.

[58] M. Wagner, I. von Harbou, J. Kim, I. Ermatchkova, G. Maurer, H. Hasse, Solubility of carbon dioxide in aqueous solutions of monoethanolamine in the low and high gas loading regions, Journal of Chemical & Engineering Data 58 (2013) 883–895. doi:10.1021/je301030z.

[59] B. Rumpf, G. Maurer, An experimental and theoretical investigation on the solubility of carbon dioxide in aqueous solutions of strong electrolytes, Berichte der Bunsengesellschaft für physikalische Chemie 97 (1993) 85–97. doi:10.1002/bbpc.19930970116.

[60] H. K. Hall, Sterically hindered phenolic buffers. application to determination of rates of amidation of ethyl chloroformate1, Journal of the American Chemical Society 79 (1957) 5439–5441. doi:10.1021/ja01577a029.

[61] A. V. Rayer, K. Z. Sumon, L. Jaffari, A. Henni, Dissociation constants (pka) of tertiary and cyclic amines: Structural and temperature dependences, Journal of Chemical & Engineering Data 59 (2014) 3805–3813. doi:10.1021/je500680q.

[62] M. Smith, J. March, March's advanced organic chemistry: Reactions, mechanisms, and structure, 6th Edition, Wiley, Hoboken, 2007.

[63] A. S. N. Murthy, K. G. Rao, C. N. R. Rao, Molecular orbital study of the configuration protonation, and hydrogen bonding of secondary amides, Journal of the American Chemical Society 92 (1970) 3544–3548. doi:10.1021/ja00715a003.

[64] V. Ermatchkov, G. Maurer, Solubility of carbon dioxide in aqueous solutions of n-methyldiethanolamine and piperazine: Prediction and correlation, Fluid Phase Equilibria 302 (2011) 338–346. doi:10.1016/j.fluid.2010.06.001.

[65] R. Notz, N. Asprion, I. Clausen, H. Hasse, Selection and pilot plant tests of new absorbents for post-combustion carbon dioxide capture, Chemical Engineering Research and Design 85 (4) (2007) 510–515. doi:10.1205/cherd06085.

[66] O. Spuhl, H. Garcia, G. Sieder, R. Notz, Comparison and limitation of different evaluation methods for novel pcc solvents, Energy Procedia 4 (2011) 51–58. doi:10.1016/j.egypro.2011.01.022.

[67] R. Notz, I. Tönnies, H. Mangalapally, S. Hoch, H. Hasse, A short-cut method for assessing absorbents for post-combustion carbon dioxide capture, International Journal of Greenhouse Gas Control 5 (2011) 413–421. doi:10.1016/j.ijggc.2010.03.008.

[68] J. Rolker, M. Seiler, New energy-efficient absorbents for the co2 separation from natural gas, syngas and flue gas, Industrial Progress 1 (2011) 280–288. doi:10.4236/aces.2011.14039.

[69] P. M. Mathias, J. P. O'Connell, The gibbs–helmholtz equation and the thermodynamic consistency of chemical absorption data, Industrial & Engineering Chemistry Research 51 (2012) 5090–5097. doi:10.1021/ie202668k.

[70] I. Kim, K. A. Hoff, T. Mejdell, Heat of absorption of co2 with aqueous solutions of mea: New experimental data, Energy Procedia 63 (2014) 1446–1455. doi:10.1016/j.egypro.2014.11.154.

[71] H. Svensson, C. Hulteberg, H. T. Karlsson, Heat of absorption of co2 in aqueous solutions of n-methyldiethanolamine and piperazine, International Journal of Greenhouse Gas Control 17 (2013) 89–98. doi:10.1016/j.ijggc.2013.04.021.

[72] D. D. Pinto, S. A. Zaidy, A. Hartono, H. F. Svendsen, Evaluation of a phase change solvent for co 2 capture: Absorption and desorption tests, International Journal of Greenhouse Gas Control 28 (2014) 318–327. doi:10.1016/j.ijggc.2014.07.002.

[73] Q. Ye, X. Wang, Y. Lu, Screening and evaluation of novel biphasic solvents for energy-efficient post-combustion co2 capture, International Journal of Greenhouse Gas Control 39 (2015) 205–214. doi:10.1016/j.ijggc.2015.05.025.

[74] P. Broutin, H. Kvamsdal, C. La Marca, P. van Os, N. Booth, A new fp7 project demonstrating co2 capture technologies, Energy Procedia 37 (2013) 6365–6373. doi:10.1016/j.egypro.2013.06.566.

[75] L. Raynal, P. Alix, P.-A. Bouillon, A. Gomez, M. F. de Le Nailly, M. Jacquin, J. Kittel, A. Di Lella, P. Mougin, J. Trapy, The dmx™ process: An original solution for lowering the cost of post-combustion carbon capture, Energy Procedia 4 (2011) 779–786. doi:10.1016/j.egypro.2011.01.119.

[76] L. Raynal, P. Briot, M. Dreillard, P. Broutin, A. Mangiaracina, B. S. Drioli, M. Politi, C. La Marca, J. Mertens, M.-L. Thielens, G. Laborie, L. Normand, Evaluation of the dmx process for industrial pilot demonstration – methodology and results, Energy Procedia 63 (2014) 6298–6309. doi:10.1016/j.egypro.2014.11.662.

[77] Y. Coulier, A. R. Lowe, A. Moreau, K. Ballerat-Busserolles, J.-Y. Coxam, Liquid-liquid phase separation of amine H 2 O CO 2 systems: New methods for key data, Fluid Phase Equilibria 431 (2017) 1–7. doi:10.1016/j.fluid.2016.10.010.

914 [78] J. Zhang, D. W. Agar, X. Zhang, F. Geuzebroek, Co2 absorption in biphasic solvents
915 with enhanced low temperature solvent regeneration, Energy Procedia 4 (2011) 67–
916 74. doi:10.1016/j.egypro.2011.01.024.

917 [79] F. Yang, X. Jin, J. Fang, W. Tu, Y. Yang, C. Cui, W. Zhang, Development of co
918 2 phase change absorbents by means of the cosolvent effect, Green Chemistry 20
919 (2018) 2328–2336. doi:10.1039/C8GC00283E.

920 [80] U. Liebenthal, D. D. Di Pinto, J. G. M.-S. Monteiro, H. F. Svendsen, A. Kather,
921 Overall process analysis and optimisation for co2 capture from coal fired power plants
922 based on phase change solvents forming two liquid phases, Energy Procedia 37 (2013)
923 1844–1854. doi:10.1016/j.egypro.2013.06.064.

924 [81] S. Ma'mun, I. Kim, Selection and characterization of phase-change solvent for car-
925 bon dioxide capture: Precipitating system, Energy Procedia 37 (2013) 331–339.
926 doi:10.1016/j.egypro.2013.05.119.

927 [82] E. Sanchez-Fernandez, F. d. M. Mercader, K. Misiak, L. van der Ham, M. Linders,
928 E. Goetheer, New process concepts for co2 capture based on precipitating amino
929 acids, Energy Procedia 37 (2013) 1160–1171. doi:10.1016/j.egypro.2013.05.213.

930 [83] S. Zheng, M. Tao, Q. Liu, L. Ning, Y. He, Y. Shi, Capturing co2 into the precipitate
931 of a phase-changing solvent after absorption, Environmental Science & Technology
932 48 (2014) 8905–8910. doi:10.1021/es501554h.